Microring Resonators and its Applications

Sauradeep Kar[a], Sridhar Singhal[a], Prasanna Paithankar[b] & Shailendra K Varshney[a*]

[a]Department of Electronics and Electrical Communication Engineering, Indian Institute of Technology Kharagpur,
Kharagpur-721 302, WB, India

[b]Department of Computer Science and Engineering, Indian Institute of Technology Kharagpur, Kharagpur-721 302, WB, India

Microring resonators (MRRs) are the most sought on-chip optical components after the optical waveguides due to versatile usages and functionalities whether in linear or nonlinear and quantum properties. A simple MRR geometry consists of one or two straight waveguides and circular or bent waveguides. Due to huge potential and versatility, we provide a comprehensive review on microring resonators that encompasses from material selection to applications and various configurations.

1 Introduction

The 21st century can be regarded as the century of Photonics while the 20th century has been considered of Electronics. Scientific community have been particularly interested to explore the field of photonics due to distinctive advantages that includes stability, scalability, compactness, and low-power consumption. Sophisticated fabrication technologies have paved the path towards development of multi-functional photonic devices in variety of material platforms. The most successful application of optical technologies has been the optical fibers after the invention of laser. Efforts have been made to explore the small dimension (μm to nm) optical devices whether is it an optical waveguide made of silicon or other materials or filters, sensors, and modulators. Over last two decades, optical microresonators is finding a huge space in research due to plethora of applications. Rudimentarily, an optical resonator is a cavity which allows light to circulate within itself in a closed path. Such resonators have been fabricated in various geometrical shapes by utilizing different materials. Micro-ring resonator (MRR) is a class of optical resonator which produce equidistant dips in the resonant spectrum at wavelengths where the phase-matching condition is fulfilled[1]. Initially fabrication technologies capable of manufacturing bulk optical resonators was developed. Spherical resonators were the first of its kind to be fabricated and found usage in micron-scale bulk optical devices[2,3]. Silica micro-spheres with high quality[4] factor, Q, were fabricated by a simple approach where the tip of an optical fiber was melt to produce a resonator. Several approaches such as electrical arc heating, laser re-flow (by usage of a CO_2 laser), hydrogen flames were utilized to produce spheroidal silica resonators with micron scale diameters[3,5–9]. Spherical resonators with smooth surfaces which are capable of suppressing scattering losses in the resonator could be successfully fabricated by the aforementioned techniques. Apart from micro-spheres, bulk resonators have also been fabricated in the disc and toroid shapes[6]. With respect to micro-spheres, micro-toroid and micro-discs have less number of degenerate modes which makes them favourable to control mode-crossing behaviour[10]. The fabrication of such resonators is via a lithographic process where a silica layer is grown on a silicon substrate followed by dry etching[6]. Resonators in the toroidal and disc shapes have shown to produce quality factor of 5×10^{810}. Complementary Metal Oxide Semiconductor (CMOS) compatible on chip MRRs have attracted researchers over many years. This is because on-chip MRRs offer huge benefits such as scalability, small footprint, improved performance and several others similar to the ones achieved in on-chip electronic integrated devices. The standard configuration of an add-drop integrated ring resonator which is used till date was proposed way back in the year 1969[11]. This basic resonator configuration has been shown in Fig. 1(a), where two straight waveguides are in close proximity with a ring waveguide, which results in evanescent coupling of

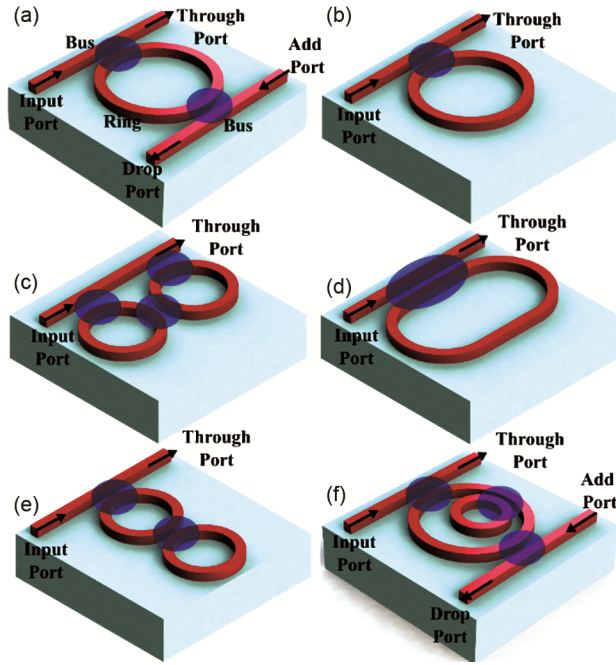*Corresponding author: (E-mail: skvarshney@ece.iitkgp.ac.in)

Fig. 1 — Schematic of on chip MRR in (a) add-drop (b) all-pass (c) Parallely coupled (d) racetrack (e) serially coupled (f) off-axis concentric coupled configuration[16]. The shaded region in the figures indicate the coupling gap(s).

the field into the ring waveguide. The shaded region in the figures indicate the coupling gap. With a single bus, the MRR configuration is referred as all-pass configuration (Fig. 1(b)). Different on-chip MRR geometries have been explored in literature which include racetrack-shaped MRR[12] (Fig. 1(d)), vertically coupled MRR[13], cascaded MRR (serial and parallel[14,15] (Fig. 1(e),(c)), off-axis MRR[16] (Fig. 1(f)), MRR with distributed Bragg grating[17] and tapered MRR[18]. Each resonator geometry has its own advantages. For instance, the coupling gap between the bus and the ring waveguides is very crucial in determining the quality of resonance. The gap can be increased by using a racetrack configuration which enlarges the coupling distance by using a straight arm in the coupling region[12]. The off-axis coupled MRR proposed in[16] has been observed to generate extra transmission dips due to phase matching between inner and outer rings, also relaxes the coupling gap between the waveguides while maintaining large extinction and high Q-factor.

1.1 Basic working principle of an MMR

As mentioned earlier, an all pass MRR consists of a bus waveguide that is evanescently coupled to a ring waveguide. Light revolves over the circumference of the ring where constructive interference occurs upon

one revolution around the ring. Thus, if β is the propagation constant and L is the circumference of the ring, then the following relation holds true[1,19]:

$$\beta L = 2m\pi \qquad \qquad \dots (1)$$

$$\frac{2\pi}{\lambda} n_{eff} L = 2m\pi \qquad \qquad \dots (2)$$

Here, m is an integer. For a MRR with a circular periphery $L = 2\pi R$, where R is the radius of the ring. At the resonance frequency light tends to get trapped inside the resonator due to which there is a dip in the transmission. The spacing between adjacent resonant frequencies belonging to longitudinal modes m and $m+1$ is known as Free Spectral Range (FSR) which is given by:

$$\Delta f_{FSR,m} = \frac{c}{n_g(\lambda_m) L} \qquad \qquad \dots (3)$$

where, $n_g = n_{eff} - \lambda \dfrac{dn}{d\lambda}$ is the group index.

The quality factor, Q, of the resonator is defined as the ratio of the energy (ξ) stored in a resonator to the energy dissipated per cycle, which is normalized to the angular resonance frequency ω_m, as,

$$Q = \frac{\omega_m \xi}{-d\xi/dt} \qquad \qquad \dots (4)$$

1.2 Analytical Modeling of an MRR

The MRR can be analytically modelled using the well-known unitary transfer matrix (U-TM) method[20,21] which helps in theoretically visualizing the transmission spectrum of a MRR. To illustrate this method, a schematic of an add-drop racetrack MRR is depicted in Fig. 2(a), where t and κ are the self- and cross- power coupling coefficients of the propagating fields in the resonator, respectively and g is the gap between the bus and the ring waveguides, L_{st} and R are the lengths of the straight arm and the radius of a MRR, respectively. The relation between the incident and reflected field phaser of the input waveguide to the transmitted and coupled field phasor of the output waveguide is given by the U-TM. The generalized U-TM can be obtained from the following expression[22,23]:

$$U = \begin{pmatrix} t & \kappa \\ -\kappa^* & t^* \end{pmatrix} = \begin{pmatrix} \cos\alpha & -j\sin\alpha \\ -j\sin\alpha & \cos\alpha \end{pmatrix} \qquad \dots (5)$$

and $\alpha \equiv KL_{eff}$, where L_{eff} is the effective coupling length which is defined as the length of the coupling region between the racetrack ring and the straight
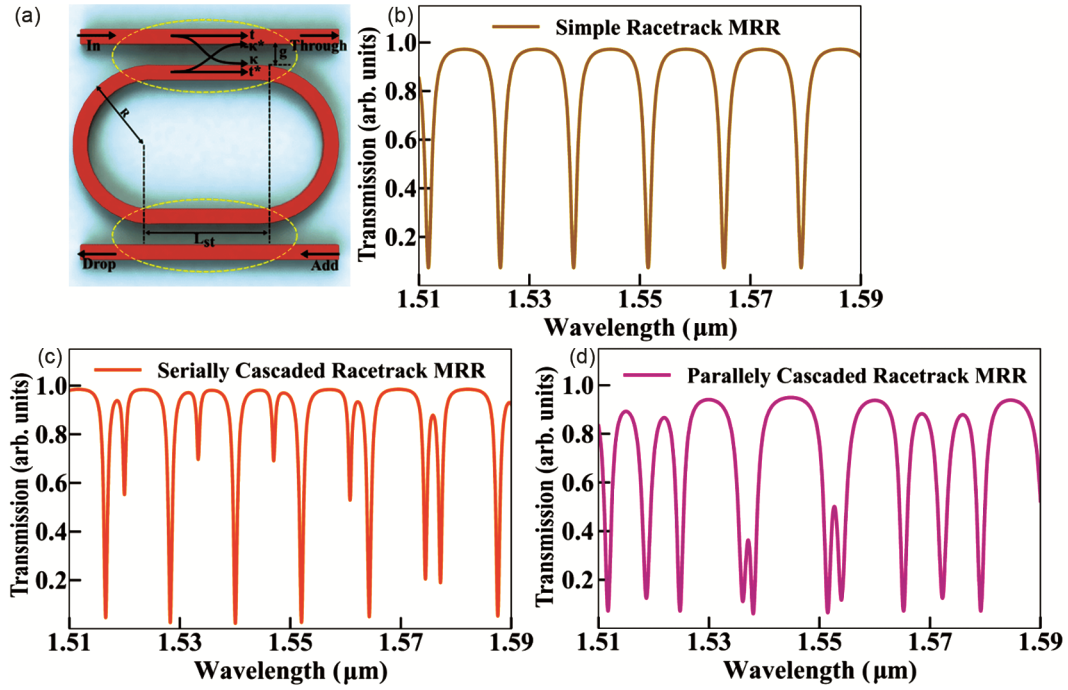
Fig. 2 — (a) Schematic of on chip add-drop racetrack MRR with indication of geometric parameters and coupling coefficients (the encircled portions indicate the coupling regions), Transmission spectra of (b) single (c) serial coupled (d) parallel coupled racetrack MRR(s).

waveguide and is determined by the straight arm length L_{st}. The factor K $= \pi/2L_\pi$, L_π is the ideal coupling length, estimated by the gap, g between the bus and the ring waveguides. The *Through* (T) and *Drop* (D) phasers are given by the following equations,

$$T = \left[t_1 + \frac{\kappa_1 \kappa_2 t_2 e^{-j\theta}}{1 - t_1 t_2 e^{-j\theta}} \right] e^{-j\frac{2\pi}{\lambda} L_{eff} n_{eff}} \qquad \dots (6)$$

$$D = \left[\frac{\kappa_1 \kappa_2 e^{-j\theta/2}}{1 - t_1 t_2 e^{-j\theta}} \right] e^{-j\frac{2\pi}{\lambda} L_{eff} n_{eff}} \qquad \dots (7)$$

The phase factor θ is given as $\theta = \Delta L \frac{2\pi n_{eff}}{\lambda}$ where, ΔL and n_{eff} are the path length traversed by the optical wave in one round-trip and the effective refractive index, respectively. The subscripts 1 and 2 denote two coupling junctions in the upper and lower branch of the MRR, respectively. For a symmetric MRR $t = t_1 = t_2$ and $\kappa = \kappa_1 = \kappa_2$. At resonance, $\theta = 2n\pi$ (n being an integer) for which ideally, the "through" and "drop" power are zero and unity, respectively. By this method, maximum through power (P_{Th}^{max}) and minimum drop power (P_{dr}^{min}) can be evaluated as,

$$P_{Th}^{max} = 4|t|^2 /(1+|t|^2)^2 \qquad \dots (8)$$

$$P_{dr}^{min} = (1-|t|)^2 /(1+|t|^2)^2 \qquad \dots (9)$$

The U-TM approach does not consider the phase difference ϕ between t and κ, which depends on the propagation length of the circulating field in the MRR and affects the resonance quality of the transmission spectrum. The information of ϕ is generally included in the "through" and "drop port" transmission phasers by considering the mode-coupling coefficients of the even and odd modes of the propagating waves. Such formulation is known as the nonunitary transfer matrix (NU-TM)[21]. Based on the above formulation, the transmission spectrum of a typical racetrack MRR with L_{st}= 10 μm and R= 5 μm has been shown in Fig. 2(b). The spectrum consists of equidistant resonant dips spaced at the FSR. The transmission spectra corresponding to serially and parallely coupled racetrack MRRs (similar to the configuration shown in Fig. 1(e) and 1(c)) has been shown in Fig. 2(c) and (d), respectively. As expected the spectra undergoes a splitting in the resonant dips due to inter-coupling of fields between multiple rings.

As mentioned earlier, the coupling of light between the bus and the ring waveguides of an MRR is a very crucial issue, and the coupling gap g mentioned in

Fig. 2(a) requires precise optimization to ensure proper operation of the MRR. Based on the field coupled from the bus to the ring waveguide, three regimes of operation of the MRR has been identified [1,20], (i) under-coupled ($t < \kappa$),(ii) over-coupled ($t > \kappa$) and critically-coupled ($t = \kappa$). Different coupling regimes are specific to various applications. For instance several nonlinear applications require the over-coupling regime[24] whereas for applications including sensing, switching, modulation and so on require the critical coupling regime.

It should be pointed in this context that the critical coupling regime yields resonances with the highest extinction. However, in general, several designs are fabricated in order to attain such critical coupling due to fabrication tolerances which stays below 5%. Such variation affects the operation of a MRR and may turn critically coupled operation into either over or under-coupled regimes. Several approaches have been proposed by researchers to overcome this vital issue, i.e. relaxing the stringent requirement of gap value. One is the usage of the RMRR configuration which has been discussed previously. The other configuration is the nested off-axis ring which has been shown in Fig. 1(f)[16,25]. As depicted in Fig. 1(f), the nested nonconcentric microring resonator (NN-MRR) consists of multiple microrings embedded into

a larger microring. A high Q-factor ($>10^5$) and a large transmission notch depth (>10dB) has been reported for the NN-MRR. The proposed resonator is compact and fabrication tolerant. The schematic representation of an all-pass NN-MRR for three concentric microrings of radii R_1, R_2 and R_3 has been shown in Fig. 3(a). The dashed rectangular boxes represent three coupling regions $CR1$, $CR2$ and $CR3$ corresponding to the junctions between the bus and the outer rings (radius R_1), the outer and the first inner ring (radius R_2), the two inner rings (of radii R_2 and R_3) respectively, τ_p and κ_p, $p = 1,2,3$ are the self- and cross- coupling coefficients at three junctions. $a_m = e^{-\alpha_m L_m/2}$, $m = 1,2,3$ are the internal loss factors of the three rings. Here, α_m, and L_m are the linear loss coefficient and the circumference of the ring(s), respectively. The semi-round trip phase change for the three rings are ϕ_1, ϕ_2, and ϕ_3 respectively. The normalized transmission at the output (i.e. through port) for such an NN-MRR configuration is given by.

$$T_3 = \tau_1 + a_1(i\kappa_1)^2(e^{i2\phi_1}\chi_1^{-1} - a_1\tau_1)^{-1} \qquad \ldots (10)$$

$$\chi_1 = \tau_2 + a_2(i\kappa_2)^2(e^{i2\phi_1}\chi_2^{-1} - a_2\tau_2)^{-1} \qquad \ldots (11)$$

$$\chi_2 = \tau_3 + a_3(i\kappa_3)^2(e^{i2\phi_2} - a_3\tau_3)^{-1} \qquad \ldots (12)$$

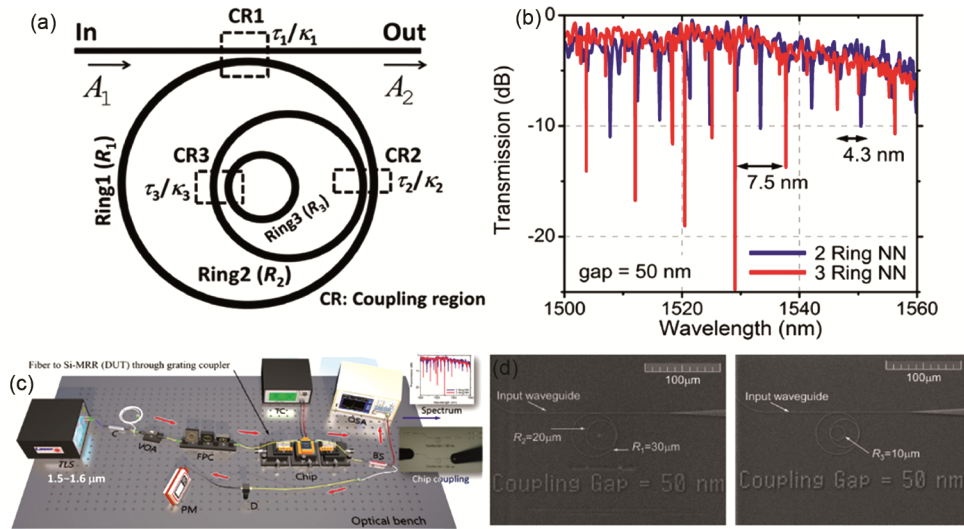The transmission spectra covering the C-band has been shown in Fig. 3(b) for gaps of 50nm between the

Fig. 3 — (a) Schematic of NNMRR with three concentric off-axis rings, $(\tau_1,\kappa_1),(\tau_2,\kappa_2),(\tau_3,\kappa_3)$ are the self and cross coupling coefficients at the three junctions CR1,CR2 and CR3. (b) Comparison between transmission spectra of NN-MRR consisting of two and three nested rings. (c) Experimental set up where light from a tunable LASER source was coupled to the NN-MRR (Device under test: (DUT)) by grating couplers; circulator (C) was used to protect the laser from back-reflection; Variable optical attenuator (VOA) and a fiber polarization controller (FPC) were used to control the input power and the polarization, respectively. The output signal was divided into two parts by a beam splitter (BS) towards a detector (D) and an optical spectrum analyzer (OSA). The output power was measured by a power meter (PM) the spectral components were recorded using the OSA. (d) Scanning Electron Microscope (SEM) image of dual and three ring NN-MRR for coupling gap of 50 nm.(Images adapted from[25])

rings for dual and three ring based NN-MRR. The FSR between resonance dips for rings of radii R_2 and R_3 were observed to be 4.3nm and 7.5nm respectively. From Fig. 3(b), mode splitting phenomena can be observed at the frequencies where resonances of the individual rings of radii R_2 and R_3 overlap. Additional notches appear due to extra phase matching because of the concentric inner rings. The experimental set-up used has been shown in Fig. 3(c) and the fabricated sample for two and three rings have been shown in Fig. 3(d).

2. Linear Applications of MRRs

On chip MRRs have been used for a plethora of linear applications ranging from couplers, filters, multiplexers, sensors and modulators. For utilizing MRRs in designing couplers, proper optimization of the coupling gap is the main requisite[26]. As evident from the transmission spectra shown in Fig. 2 (b), the sharp dips at the resonant frequency makes MRR effectively act as a notch filter. When a double ring resonator is used as a wavelength drop filter, switching of the resonance between the ON and OFF state becomes possible by detuning the rings with respect to one another. Such an MRR has been used as a wavelength-selective switch[27]. Modulation is typically brought about by change in refractive index and can be divided into electro-refractive or electro-absorptive modulators depending on whether the change is being brought in real or imaginary part of the refractive index. Precise control of absorption directly modulates the intensity of propagating signal, which is the case in electro-absorptive modulators. For the electro- refractive scenario, change in refractive index is converted to intensity modulation through two types of devices, (1) interference using Mach-Zender interferometer (MZI) and (2) resonator-based devices, which exhibit change in the resonant condition due to change in refractive index.MZI based modulators due to large footprint gives rise to higher insertion loss, power consumption, device area and difficulty to integrate on-chip. On the other hand, MRR based devices are reasonably compact, CMOS compatible, low power consumption, and hence proven to be efficient in realizing optical modulators[28]. Modulation in case of MRR based modulators can be brought either by change in temperature[29] or change in the geometry[30,31]. Since modulators are key components of communication systems and optical processors[32], it is necessary to

realize energy efficient, compact, and low loss modulators. Thermal and geometrical modulation provide lower losses and smaller footprint as compared to carrier injection-based device[33], but the attained modulation speeds are slow[34,35]. It has been reported[36,37] that the usage of NNMRR (detailed in the last section) with sharp transmission notches aid in realizing athermal CMOS-compatible modulators. In this review, usage of MRRs for filters and sensors have been elucidated in detail.

2.1 MRR as Optical Filters

The foremost principal application of MRR lies in the development of optical filters. Rudimentarily, a filter can be defined as a device that can alter the amplitude and phase of a signal in a particular manner. Lower radiation losses, small footprint, high Q-factor make MRR based devices attractive in construction of compact channel filters for Wavelength Division Multiplexing (WDM) system. Generically, filters can be classified as Finite Impulse Response (FIR) and Infinite Impulse Response (IIR) filters. As the name suggests, the impulse response $h(t)$ of FIR filters stays for a finite duration of time whereas it continues indefinitely for IIR filters. Researchers have realized FIR optical filters by directional couplers and Mach-Zender interferometers[23,38]. IIR filters require a feedback mechanism for the sustenance of the impulse response over a prolonged duration. The positive feedback in the MRRs make them suitable for designing IIR filters.

The z-transform analysis has been useful in the generalized analysis of spectral response of ring resonator filters. The unit variable z^{-1} denotes the round-trip phase delay of the resonator. For an add drop MRR, the simplified schematic for z-transform analysis is shown in Fig. 4(a) and 4(b). The transmission at the drop port can be obtained by the generic transfer function in the z-domain as,

$$H_{21} = \frac{E_{t2}(z)}{E_{i1}(z)} = \frac{-\kappa_1 \kappa_2 \sqrt{\alpha z^{-1}}}{1 - t_1 t_2 \alpha z^{-1}} \qquad \ldots (13)$$

Subsequently the scattering matrix in the z-domain which links the input and output ports, is given by the following expression,

$$\begin{pmatrix} E_{t1}(z) \\ E_{t2}(z) \end{pmatrix} = S_{RR}(z) \begin{pmatrix} E_{i1}(z) \\ E_{i2}(z) \end{pmatrix} \qquad \ldots (14)$$
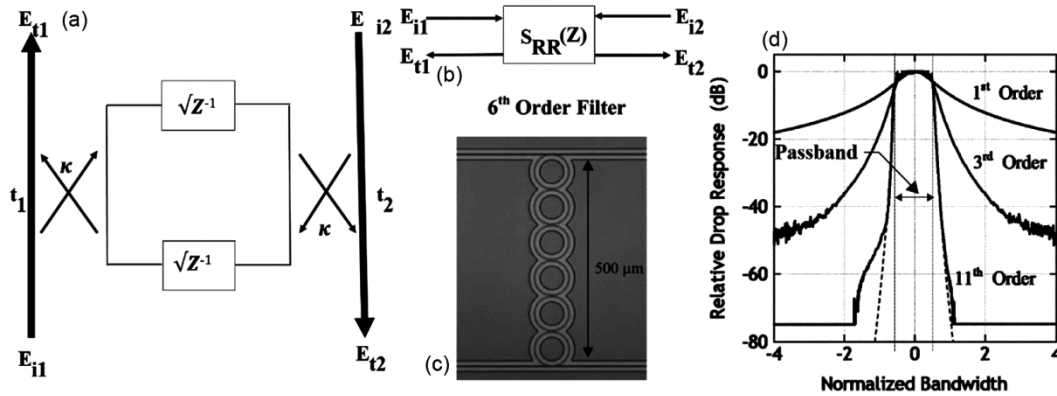
where,

Fig. 4 — (a) z-domain model of the add-drop MRR, the total round-trip phase delay gets denoted by the variable z^{-1}, (b) Two-port z-model of add-drop MRR , the matrix $S_{RR}(z)$ is the scattering matrix in the z-domain which links the signals at the input and output ports. (c) Schematic of a 6th order cascaded add-drop filter, (d) Figure illustrating sharp roll off between the pass and stop band for an 11th order filter compared to a 3rd and 1st order filter[39].

$$S_{RR}(z) = \begin{pmatrix} \dfrac{t_1 - t_2\alpha z^{-1}}{1 - t_1 t_2 \alpha z^{-1}} & \dfrac{-\kappa_1\kappa_2\sqrt{\alpha z^{-1}}}{1 - t_1 t_2 \alpha z^{-1}} \\[3mm] \dfrac{-\kappa_1\kappa_2\sqrt{\alpha z^{-1}}}{1 - t_1 t_2 \alpha z^{-1}} & \dfrac{t_2 - t_1\alpha z^{-1}}{1 - t_1 t_2 \alpha z^{-1}} \end{pmatrix} \quad \dots (15)$$

The general form of the transfer function of a digital IIR filter in the z domain is given by,

$$H(z^{-1}) = \frac{P(z^{-1})}{Q(z^{-1})} = \frac{K_0 \prod_{k=1}^{M}(z^{-1} - z_k)}{\prod_{k=1}^{N}(z^{-1} - p_k)} \quad \dots (16)$$

here, $P(z^{-1})$ and $Q(z^{-1})$ are polynomials of z^{-1}, and z_k and p_k are the zeros and poles respectively in the inverse z-plane.

For designing an MRR based optical filter, the specification of the desired transfer function H is done in the z-domain. The location of the poles and zeros are chosen to achieve specific amplitude and phase characteristics of the filter. After deducing the transfer function, a suitable MRR configuration and its coupling coefficients are determined to deduce the spectral response. This method is referred as filter synthesis problem[19]. The Lorentzian response of single resonating ring can be modified by a cascade of coupled rings to obtain higher-order filter characteristics[40], a flat pass band may be obtained for a coupled system consisting of infinite number of resonators[41]. Higher-order filters can provide the suitable pass band response along with sharper roll-offs and higher attenuation in the stopband[42,43]. However, reflections at waveguide and resonators lead to ripples even for 100 coupled resonators[44] The ripples can be mitigated by tapering the inter-

resonator coupling coefficients [39,45]. Since the spectral response is narrow and box like for higher order filters, it is possible to drop out single frequency provided the free spectral range covers the entire C-band about 35nm, which is possible for rings of size about $2.5\mu m$[46]. Fig. 3(d) shows that the filter response precisely becomes box-like with sharp roll-off between the pass and the stop band as the order of the filter is increased from 3 to 11, or in other words when the number of cascaded rings is increased. Also, it has been possible to achieve[47] tuneable range throughout the C-band which fulfils the one device fits all notion.

While a good ring resonator could well meet the requirements for a WDM system, in some circumstances, it may lack in tolerance to variations in fabrication and environmental changes (e. g. temperature). This is particularly prevalent in silicon-based systems, where resonance frequencies in microrings are very sensitive to temperature shift due to the high thermo-refractive coefficient of Si[48].To accommodate temperature and fabrication variations, widening the bandwidth of the filter has been proposed as a remedy, the width being adjusted by tuning inter-resonator coupling strengths[49]. However, this technique would not be applicable to WDM applications as they require a narrow bandwidth. While[50] presents techniques to resolve this temperature dependence in Silicon MRR devices, converting the problem of temperature dependent resonance wavelength as an opportunity,[51,52] propose stabilised filters involving heaters for controlling resonance wavelengths, also providing tolerance to fabrication errors[20,53].A wide FSR is requisite for

precise filtering of the passband which maybe spanned over a broad continuum of frequencies. If resonance dips are closely spaced, the pass band of the filter designed from such an MRR would naturally be very small. It is clearly visible from Eq.3 that FSR of MRR is inversely proportional to the radius of the ring. However, smaller bend radius increases fabrication complexity, reduces quality factor of resonance, introduces losses which increase rapidly as the radius reduces[54,55] and can lead to polarization effects as well[56].

By altering the dimensions of the cascaded rings in higher-order filters, it is possible to suppress unwanted resonances through the Vernier effect[57,58]. For a microring resonator system consisting of two resonators, the total FSR can be obtained using,

$$FSR_{tot} = N.FSR_1 = M.FSR_2 \qquad \dots (17)$$

where N and M are natural numbers which are relatively prime to each other[59], with one such number for each closed loop,[60,61]. For example[62] used two large rings of individual FSRs of 8 nm and 6 nm respectively to obtain a total FSR of 20nm. Researchers have been successful to achieve FSR surpassing the C-band easily[15,63–66] by this technique. However, including multiple rings in Vernier configuration require high precision and fabrication tolerance. Multiple ring configuration also suffers from poor tuning efficiency. Another method used widely involves utilisation of a reflection element in the ring, producing waves in direction opposite to the original one. Gold nano-disks[67] as the reflecting elements to obtain wider FSR has been used, whereas reported an MRR with Sagnac loop to enhance Q factor and FSR[68]. Introducing new structures will increase fabrication complexities and impact density of integration. It has been recently[69] pointed that two Fabry-Perot (FP) cavities, made by introducing gap in the straight arm of the RMRR which can successfully produce a wide FSR.

2.2 MRRs for Sensing Applications

On-chip MRRs have been vastly exploited for sensing applications. The applicability of MRRs for sensing purposes stems from the basic relation given in Eqn. (3) where, resonance wavelength is proportional to the ring radius and effective refractive index. So, any perturbations provided to the system, through change in surrounding refractive index, temperature, or injecting carriers in the ring through electro or all optical methods (pump) will lead to change in the effective refractive index Δn_{eff} and hence the resonance wavelength $\Delta\lambda$, which can be computed by the following generalized relation:

$$\Delta\lambda = \frac{\Delta n_{eff} L_C}{m} \qquad \dots (18)$$

where m is a natural number, L_C is the circumference of the ring. This equation can be written as a linear function of change in cladding refractive index (environmental change), δn_{ev},

$$\Delta\lambda = \frac{\delta_{ev} n_{eff} \lambda}{n_g} \qquad \dots (19)$$

where, $\delta_{ev} n_{eff}$ is the change in effective refractive index due to change in environment. The change in output response of the MRR due to environmental change can be detected by two schemes: resonant-wavelength-shift and intensity variation scheme. A shift in resonance wavelength is obtained from the spectral measurement of the output optical signal, which requires sophisticated and expensive setup. On the contrary, intensity-variation can be easily measured through photo detectors. Since MRRs produce high Q resonances (*i.e.* resonant dips with high extinction), the slope of intensity variation with wavelength is very steep near the resonance wavelength of an MRR. This translates to a large change in detected intensity. Hence, this scheme is easily realizable through simple and inexpensive experimental setup and provides higher sensitivity. However, the intensity variation-based systems have a smaller dynamic range[70–72]. Any sensor must possess high resolution, so that it can detect small concentration of sample as samples may often contain contaminants hindering detection. Various detection techniques have been developed such as fluorescentlabel-based technique, electronics, Quartz Crystal Microbalances (QCM) and optical techniques. Optical methods have been widely explored for advantages of fast detection, strong light-interaction, high sensitivity and on-chip integrability, of which the MRR based technique is particularly useful. For sensing of fluids (in chemical and bio sensors), the mechanism can be divided into two categories depending on the mechanism of obtaining light signal from the chemical domain: homogeneous sensing and surface sensing. In homogenous sensing, the analyte is disposed over the entire resonator, which leads to a change in the effective refractive index, and a corresponding shift in the resonant wavelength.

The sensitivity is defined as, $S = \Delta\lambda/\Delta n_{ev}$. However, this method is incapable of effectively differentiating between different kinds of analytes. In surface sensing, receptive materials are placed over the surface of the resonator[73], which bind with specific analytes. Surface sensing is widely used in biological sensing and diagnostics[74–76]. Based on similar principles, researchers have developed sensors based on MRRs for detection of many chemicals such as, gases bio-toxins and microorganisms[77] *etc*. The procedure adopted by researchers for detection of some analytes have been summarized in Table 1. Here LOD denotes Limit of Detection which is defined as the lowest concentration of the analyte that can be detected by a sensor. For single nano-particle detection, many label free techniques have been investigated, such as Surface Plasmon Resonance (SPR) imaging[94], Photonic Crystal Fiber (PCF) enhanced microscopy[95], interferometric microscopy[96]. Many of these techniques are also ailed by low interaction between particle and light, which is the bottleneck of MRR based sensing. In micro-cavities, light circulates multiple times before its decay due to losses, which allows light to interact multiple times

with the target material which produces a significant change in output signal and facilitates effective sensing behaviour. Various resonator geometries such as sphere[97], ring[98], MRR coupled with cavity[99] have been proposed. While MRR have excellent advantages of high Q factor, high sensitivity, ease of integration in CMOS, in conventional silicon based MRR, due to high refractive index contrast, the evanescent field is low resulting in poor interaction with the surrounding medium. Therefore, it is necessary to increase the magnitude of the evanescent field spilling out from the core by geometrical modification of the MRR.[100] proposed a tapered (RMRR) for detection of metallic nanoparticles. A photonic nanofence (PNF), i.e. a ridge waveguide of sub-wavelength dimensions is connected to the tapered RMRR waveguide (Fig. 5(a)). As the dimensions are much smaller than the conventional input and output waveguides, field is pushed outside the waveguide boundary, thus enhancing evanescent field. Increase in evanescent field means higher radiative losses, which by definition implies a reduction in Q-factor. For this reason, the dimensions of the PNF have been optimized (Fig. 5(b)) to produce

Table 1 — Strategies adopted by various researchers for sensing by MRRs
(Abbreviations used: MZI: Mach-Zender Interferometer, LOD: Limit of Detection, CFU: colony forming unit)

| Analyte	Strategy	Experimental Results	Year	Ref
Hydrogen	Si MRR enhanced MZI with Pt-WO₃ receptor	0.1% vol. LOD	2019	[78]
Ammonia	Graphene clad Si MRR, change in Fermi level (and absorption) of graphene due to NH_3	Adjustable 0.5 ppm to 1000 ppm(0.1%) LOD	2019	[79]
Ethanol	SOI MRR with nanocrystallineZnO film receptor	100 ppm LOD	2010	[80]
Methane	SOI MRR with high evanescent field waveguide, intensity detection	20.8 ppb LOD	2017	[81]
VOCs	SOI MRR with poly(2-vinyl pyridine) receptor	5ppm LOD	2018	[82]
CO_2	SOI MRR with PbSe Quantum Dots deposited in core	10 ppm LOD	2021	[83]
TNT	Sol-gel imprinted polymer MRR for enhanced adsorption of TNT	5 ppb LOD High sensitivity 1pm/ppb	2019	[84]
Lead & Mercury	Mesoporous silicate coatings on SOI waveguide for trapping Heavy metal ions	100 ppb LOD	2015	[85]
Cadmium	RMRR with Ligand based receptor	38.9 ng/L LOD	2019	[86]
DMMP	SiN MRR with Polymer cladding receptor, acting as chemo-selective sorbent to DMMP molecules	2 ppb LOD	2014	[87]
Ricin	Si MRR with Sd Abreceptor	300 pMolar LOD	2013	[89]
Testosterone	Molecular Imprinted Polymer cladding over SOI MRR	48.7pg/mL LOD	2015	[90]
E.Coli	Vertically coupled Si MRR with, antibodies and single DNA oligonucleotides based surface receptor	10^5 CFU/ml LOD	2008	[73]
Salmonela	SiO₂-TiO₂ MRR, embedded in flaggelin layer as receptor for binding bacteria	7×10^{-4}RIU LOD	2016	[91]
Bean-Pod Mottle Virus	SOI MRR, coated with perfluoro plymer functionalised with antibodies	10 ng/ml LOD,	2012	[92]
Pathogen Biomarkers	Si MRR based detection of glycol-proteins for multiple viruses, activation using multiple antibodies	10 ng/mL to 39 ng/ml LOD	2015	[93]
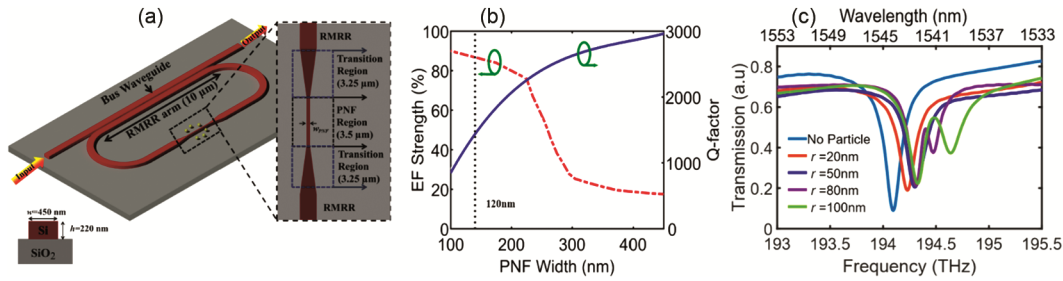
Fig. 5 — (a) Schematic of PNF assisted RMRR for single nanoparticle detection made on SOI connected via tapered waveguide, (b) Increase in Evanescent Field strength and reduction in Q factor due to introduction of PNF, (c) Output characteristic of the sensor for Gold nanoparticle detection of various sizes (*r*). (Images Adapted from[100])

proper Q-factor. A four-fold increase in evanescent field (EF) has been reported along with well-defined Lorentzian-shaped resonant dips having a Q-factor of 1400. The geometry proposed, generates three crucial modifications in the output signal, (1) Shift in Resonance spectrum due to change in refractive index in presence of nanoparticle, (2) Mode Splitting due to backscattering of light from nanoparticle that couples back into the resonator, lifting degeneracy, (3) Reduced power due to light scattering and absorption from the nanoparticle, as shown in Fig. 5(c).

Besides changes in the cladding, any perturbations to the microring structure either explicitly introduced, or due to change in environment will also lead to change in the resonance characteristics. Resonance frequencies in microrings are very sensitive to temperature shift[48], and have been used widely to make temperature sensors. Recent publications use combination of materials or design strategies to improve the response with temperature.[101] uses photonic crystal based MRR. Since, Si has a larger thermos-optic coefficient as compared to other materials like SiN, silica, it has been effectively used in designing temperature sensors.[102] has reported a sandwiched silicon – silica structure which can be potentially used for temperature sensing.[103] showcases a SiN waveguide with Liquid crystal cladding to increase interaction with temperature.

Similarly, alterations to dimension and shape of MRRs facilitate design of opto-mechanical sensors from resonators.[104] proposed a strain sensor based on flexible polymer substrate, using MRR excited at 1310nm. The same group [105] developed a MRR based accelerometer and has reported sensitivity over an order higher than commercially available (Micro-Electro-Mechanical Systems) MEMS devices. Ultrasonic sensors based on MRRs have also been proposed[106,107], which are developed for medical (endoscopy)[108] and photo acoustic microscopy applications[109].

3. Nonlinear Applications: Kerr Frequency Comb

Optical micro-resonators possess the unique ability to store and enhance the optical field circulating inside it. Due to this reason, MRRs have the capability of exhibiting nonlinear optical phenomena at reasonably low input powers which would otherwise require typically high-power optical pump sources. The interplay between several linear (like round-trip loss and chromatic dispersion[1]) and nonlinear (like self-phase modulation, cross-phase modulation, modulational instability and four wave mixing (FWM)[110]) effects occur within the MRR while the optical field circulates within it. This can lead to the formation of equidistant frequency lines in the spectral domain which are conventionally named as Kerr Frequency Combs (KFCs)[111,112]. Such KFCs manifest as temporally localized ultra short pulses, that are commonly known as Dissipative Kerr Solitons (DKSs)[113,114]. DKSs are similar to traditional solitons formed in optical fibres and waveguides[115] with an additional continuous wave (CW)) background in their temporal signature[116]. The input pump signal that is applied at the bus waveguide of the MRR finally manifests as the (CW) background in the temporal profile of the DKS. The perspective view of the three-dimensional projection of a DKS and a schematic representation of a KFC has been depicted in Fig. 6(a & b) while (c) indicates the toroidal resonator platform for generating KFCs. On-chip MRR based KFCs are inherently robust in nature[117–119]. Due to this reason KFC generation using MRRs have been attracting researchers for the past decade as an alternative to frequency comb sources based on mode-locked femtosecond lasers. MRR based KFCs encompass a wide range of applications which include development of optical atomic clocks with unparalled stability[120,121], optical frequency synthesizers[122,123], generation of microwave frequency signals with
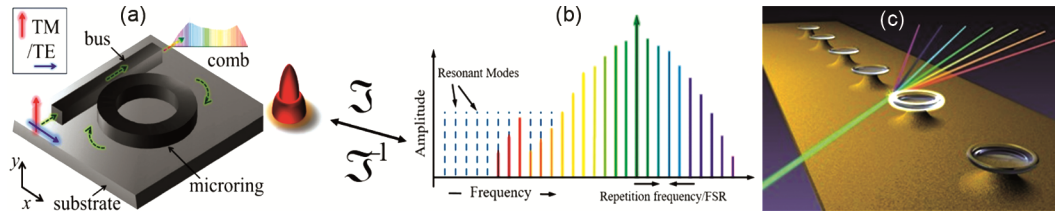
Fig. 6 — (a) Schematic representation of single DKS state generated in the on-chip MRR platform in the temporal domain which forms a Fourier Transform pair with (b) KFC in the spectral domain (c) KFC generated from micro-toroid resonator.

low phase noise[124]. MRR based KFCs have exhibited the potential to serve as a new class of novel light source for spectroscopic applications[125]. The first demonstration of on chip micro-comb sources occurred in 2010 by two independent groups[126,127] with the added benefits of reduction in cost, footprint, and energy consumption. Since the development of coherent super continuum sources[128] the generation of resonator-based KFCs have already been taking place at a rapid pace, subsequent question on the phase coherence of the generated KFC became a central issue. The investigation of the coherency of KFCs had been first carried out in 2011[129]. Thereafter, on-chip MRR based KFCs spanning over a wide spectral range of an octave has been demonstrated in literature[130,131]. The bandwidth of such KFCs is generated through Kerr-mediated FWM, and stability is achieved through nonlinear self-organizing processes.

Silicon-on-Insulator (SOI) initially appeared to be an attractive platform to realise on-chip MRRs and hence integrated micro-combs. Silicon (Si) has been quite useful to manifest third-order nonlinear optical effects, like self-phase modulation, cross-phase modulation and FWM[132]. Si possesses substantially high Kerr nonlinearity (n_2) which along with the high refractive index contrast in SOI based devices facilitates tight confinement of light within such devices. This inherently leads to a high nonlinear parameter (γ) in SOI devices ($\gamma = \omega n_2 / c A_{\text{eff}}$, where c is the speed of light and A_{eff} is the effective mode area). Several fascinating nonlinear optical phenomena such as time lensing[133], optical regeneration[134], slow light based signal processing[135], Raman lasing[136], parametric gain[137–141] have been successfully demonstrated in SOI platform. Despite the advantages enlisted earlier, there are two crucial issues with SOI that cause a major hindrance to successful KFC generation particularly in telecommunication band (C-band) especially around 1.55μm. First, the absence of centro-symmetry abrogates all second-order nonlinear optical effects in SOI based devices. The second and the most serious issue is the presence of nonlinear losses like multiphoton absorption in the telecommunication band, which arises because the indirect bandgap energy of Si at such wavelengths is well below the multi-photon absorption (MPA) energy. KFC sources in Si MRR has been successfully demonstrated in the Mid-Infrared (MIR) frequency band (between 2μm and 6 μm)[142,143] where MPA vanishes. A comprehensive theoretical study of the dynamics of KFCs and DKS states in presence of nonlinear losses such as MPA, free-carrier absorption, and free-carrier dispersion has been reported in[144]. Due to the high MPA, several alternative CMOS compatible platforms have been used to fabricate MRRs to successfully generate KFCs in the communication wavelength(s) (around 1.55 μm). These include silicon nitride (Si_3N_4), silicon oxinitrides (SiO_xN_x) and Hydex glass[145]. Such platforms tend to have low linear loss and relatively large nonlinearities compared to standard optical fibers but possess the distinctive advantage of low nonlinear losses at the communication wavelength[146]. Furthermore, CMOS compatibility, high material stability and ease with which dispersion can be tweaked[126] makes such platforms highly suitable for fabricating MRRs. The past few years have seen remarkable progress in usage of such platforms in order to study the dynamics of KFCs in MRRs. The first demonstration of KFC in Si_3N_4 and Hydex took place in 2010[126,127]. In MRRs fabricated from such platforms, KFCs possessing a very wide spectral bandwidth spanning over an octave or more[130,131,147], on chip KFCs with a 100 GHz spacing between the different frequency components[148] have been reported. In addition, phase coherent mode-locked KFCs generated from 200 fs solitonic pulses has been reported in[149]. Also, KFCs generated from single and multiple DKS states which are controllable through the detuning between the input pump laser and the MRRs resonance mode had first been comprehensively studied through experiments in[150]. A

novel method for generation of coherent mode-locked KFC in an on chip Si_3N_4 resonator has been proposed in[151]. This scheme of filter driven FWM has successfully produced broadband KFC with frequency components having small line width of 130kHz. This scheme has been illustrated in Fig. 7 (a) and (b). The KFCs and the corresponding temporal signatures for different input powers have been depicted in Fig. 7(c) and (d). Dual KFCs which get manifested because of multi-soliton pulse generation has been reported in[152]. Second harmonic generation in Si_3N_4 has been studied through high-Q MRR based on-chip KFC[153].

Truly such breakthrough in nonlinear optical studies in MRRs have been possible because of the aforementioned material platforms like Si_3N_4. Still, the fabrication of Si_3N_4 based MRRs have always remained challenging. The major difficulty has been to grow low loss layers of Si_3N_4 with a thickness more than 250 nm. Such thickness is required for adequate mode confinement and dispersion engineering which is crucial for nonlinear applications. Si_3N_4 films contain residual hydrogen which is a major source of loss at communication wavelengths. For this reason, such films need to be annealed at very high temperatures to eliminate the residual

hydrogen. Plasma enhanced chemical vapor deposition (PECVD) and low-pressure chemical vapour deposition (LPCVD) techniques[126,154] have successfully generated thick Si_3N_4 layers with low propagation loss which are easily amenable for nonlinear applications. Further, the tensile film stress of Si_3N_4 is intrinsically high which causes a major hindrance to adequate optical confinement within the ring resonator and hence limits its quality (Q) factor.

The stress in Si_3N_4 films have been overcome by introducing mechanical trenches within the ring[155] thereby shooting up the intrinsic Q-factor to 7 million. Dispersion engineering in a Si_3N_4 MRR with 50 μm radius has been reported through conformal coating of the Si_3N_4 waveguide by HfO_2[156] as shown in Fig. 8(a). Tweaking of magnitude and bandwidth of the regime of anomalous dispersion through a change in the thickness of HfO_2 coating has been reported in this work. Fig. 8(b) shows the change in the dispersion and the zero-dispersion wavelength of the waveguide upon tweaking the thickness of the HfO_2 coating. Engineering the dispersion of Si_3N_4 waveguides has also been used as an important tool in[157,158] to stretch the bandwidth of the generated KFC. The change in dispersion profile by tweaking the dimension of the
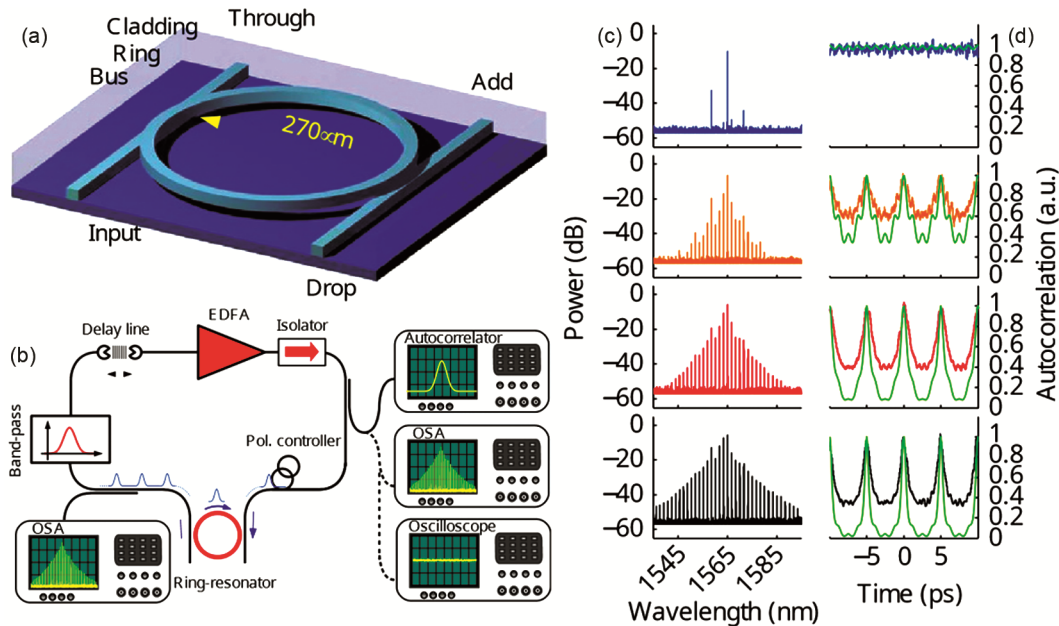

Fig. 7 — (a) Schematic of high index integrated doped Silica glass four-port MRR. (b) Experimental schematic of the "Filter-driven FWM" scheme. The loop cavity encapsulating the MRR in (a) comprises of a active-gain fibre (EDFA), a band-pass filter for signal conditioning of the pump wavelength, the delay-line controls the phase of the loop cavity modes with respect to the modes of the MRR, an isolator, and a polarization controller. The auto-correlator measures the pulse duration, the optical spectrum analyser (OSA) measures the output spectrum.(c) Loop cavity spectral signature for increasing (top to bottom) pump powers, achieved through 5.5 (blue), 28 (orange), 40 (red) and 68mW (black) average ring input powers. (d) Temporal waveform of the laser measured with the auto-correlator. (Images adapted from[151])
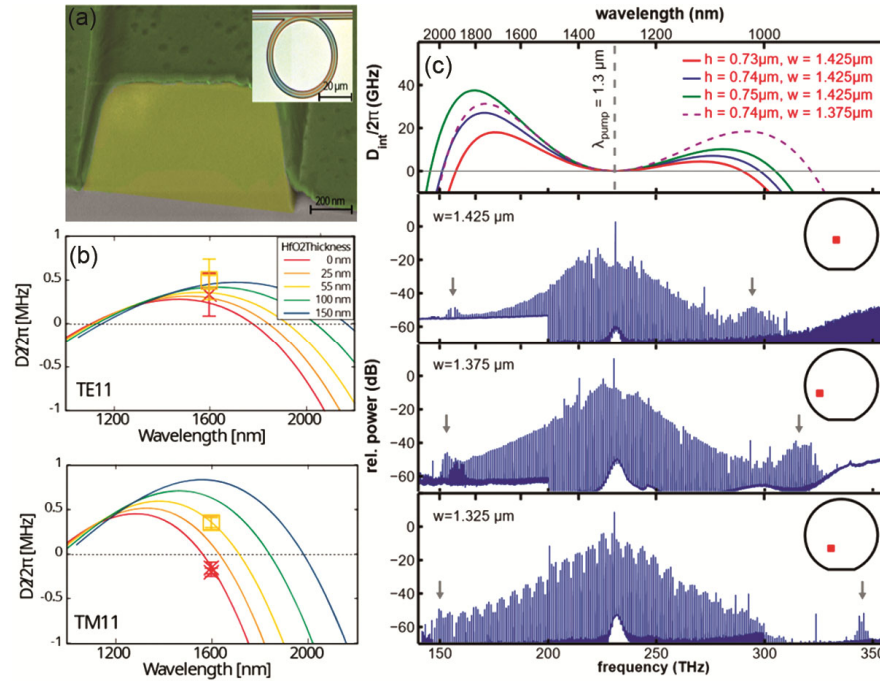
Fig. 8 — (a) HfO$_2$coated Si$_3$N$_4$ waveguide[156], (b) change in the HfO$_2$ thickness brings about a change in the bandwidth of anomalous dispersion[156], (c) (Top) Simulated integrated dispersion ($D_{int}(v)/2\pi$)of Si$_3$N$_4$ MRR for different waveguide height, h and width, w[158], (bottom) KFCs whose bandwidth can be tweaked via dispersion engineering. The arrow positions indicate dispersive wave emissions[158] (dispersive waves (DWs) triggered by higher order dispersion are emitted at the zero-dispersion wavelength because of the efficient phase matching condition[110]).

Si$_3$N$_4$ waveguide which results in varying KFC bandwidth(s) as reported in[158] has been depicted in Fig. 8(c). Si$_3$N$_4$ based integrated MRRs typically have small footprints with FSRs in the GHz regime. Several innovative MRR geometries have been proposed[159] to tweak the FSR of the microring and hence modulate the frequency spacing between the individual comb lines. Such geometries have yielded KFCs with two distinctive spectral signatures. One, in which the initial sideband of the KFC is separated from the pump by a single FSR spacing (termed as "Type I" KFC), and the second, in which the initial sideband is separated from the pump signal by several FSRs (termed as "Type II" KFC). In[160] the intracavity field dynamics near the avoided mode crossing point has been theoretically studied in a *Si$_3$N$_4$* based concentric MRR. Recently Gallium Phosphide (GaP) - on Insulator (GOI) is being explored for fabricating MRRs for nonlinear applications[161]. In addition to possessing a wide transparency range (0.55μm to 11μm), GaP has negligible nonlinear loss above 1.1μm. Along with an appreciable third order nonlinear coefficient χ^3 it possesses a reasonably high second order nonlinearity χ^2, which facilitates spectral spread of the KFC through second harmonic generation and parametric down conversion process. Multi-color KFC in the spectral windows of 1.55 μm and 3.1 μm have been reported in a GOI waveguide based MRR[162]. The GaP-OI MRR consists of a trench of dimension 250 nm × 410 nm within a 600 nm × 2990 nm waveguide. The trench facilitates a 3.25μm wide anomalous dispersion profile which facilitates the generation of broad multi-chromatic KFCs. AlGa As-OI waveguides have also proved to be very effective in fabricating MRRs for nonlinear applications[163].

3.1 Theoretical modelling of MRR based KFC

In a rudimentary form the dynamics of MRR based KFCs can be theoretically understood by the approach of coupled mode theory[165]. This methodology evaluates the resonant frequencies of the different eigen-modes of the resonator and takes in account the temporal dependence of the modal amplitudes. The cavity dispersion and effective mode volume are evaluated by a set of ordinary differential equations to trace the temporal dynamics of each participating longitudinal mode corresponding to each frequency component within the KFC. Although the coupled mode formalism is physically accurate but the process involves tedious analytical calculations and remains

incapable to provide generalized guidelines to explore the frequency comb dynamics in MRRs both temporally and spectrally. As an alternative to the coupled mode analysis, the usage of a generalized mean field equation has proved to be convenient and efficient to comprehensively describe the subtle dynamics of KFCs in the temporal and spectral domains through semi-analytical approximations. The commonly used mean field model to theoretically realize KFCs in MRRs is the "Lugiato-Lefever equation" (LLE)[166]. In order to arrive at the LLE the famous equations described by Ikeda[167,168] proves to be particularly useful. These set of equations which are collectively known as the "Ikeda Map" comprehensively describes the light transmission within nonlinear ring cavities by applying the slowly varying envelope approximation (SVEA) of the propagating electric field into the well-known Nonlinear Schrodinger Equation (NLSE)[110]. The field dynamics inside the MRR gets described by two steps with this technique. Firstly at the onset of each round-trip within the ring the intra-cavity field gets exposed to cavity boundary conditions due to the losses of the

input coupler along with the addition of the input CW pump field (see Fig. 9(a)). Thereafter, the resultant field evolution is studied over a single roundtrip circulation within the MRR when acted upon by chromatic dispersion and Kerr nonlinearity. The following equations of Ikeda Map holds true,

$$E^{(m+1)}(0,\tau) = \sqrt{\theta}E_{in} + \sqrt{1-\theta}E^{(m)}(L,\tau)e^{i\varphi_0} \quad \dots (20)$$

$$\frac{\partial E(z,\tau)}{\partial z} = -\frac{\alpha}{2}E + i\sum_{k\geq 2}\frac{\beta_k}{k!}\left(i\frac{\partial}{\partial\tau}\right)^k E + i\gamma|E|^2 E \quad \dots (21)$$

$E^{(m)}$ represents the circulating intra-cavity field in the mth roundtrip. z is representative of the longitudinal propagation coordinate. τ is representative of a reference frame which moves at the group velocity. θ denotes the power coupling coefficient of the input coupler, $L = 2\pi R$ represents the longitudinal distance traversed by the circulating field upon each roundtrip which is numerically equal to the circumference of the resonator. ϕ_0 indicates the phase accumulated by the circulating field upon each roundtrip with respect to the phase of the input pump field. α is the absorption coefficient of the resonator.
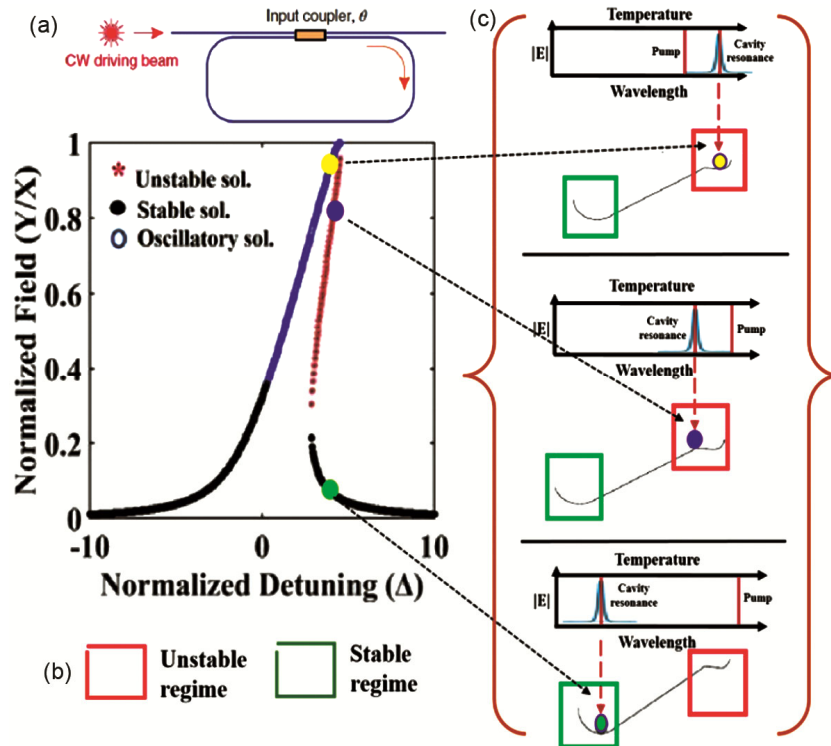

Fig. 9 — (a) Basic schematic of MRR which is used to model the Ikeda Map, (b) Kerr tilt curve from the Homogeneous steady state analysis of a CW pumped conventional MRR (parameters used from164). Stable, Unstable and oscillatory solutions are denoted by black circles, red asterisk and blue circles respectively. The DKS in the three solution regimes are denoted by yellow, violet and green circles. (c) The DKS solutions in the stable and unstable regimes of operation corresponding to which, there is a change in cavity temperature because of the detuning has been depicted with the aid of a cartoon diagram.

β_k represents the Taylor series expansion of the propagation constant $\beta(\omega)$ with respect to the angular frequency of the CW driving field (ω_0). Clearly β_2 represents the second order group velocity dispersion (GVD). γ is the nonlinear coefficient of the resonator. Eqn. (6) is the general form of the NLSE[110]. In an MRR the DKS formation takes place upon multiple roundtrip circulation of the intra-cavity field over the resonator's circumference. In such a scenario Eqn. (5) and (6) gets averaged into a single externally driven and damped NLSE which is the LLE[169],

$$t_R \frac{\partial E(t,\tau)}{\partial z} = \left[-\alpha - i\delta_0 + iL\sum_{k\geq 2}\frac{\beta_k}{k!}\left(i\frac{\partial}{\partial\tau}\right)^k + i\gamma L|E|^2 \right]E + \sqrt{\theta}E_{in}$$

... (22)

In this equation t_R denotes the round-trip time and δ_0 is the phase detuning of the cavity resonance with respect to the pump resonance mode. The variable $t = mt_R$ represents the slow time or the time scale requisite for the intracavity field to converge to a stable DKS over m roundtrips. The LLE can be solved numerically, and the different classes of solutions provide a deep insight into the temporal and spectral behaviour of the KFC and is also capable of analyzing the stability of the comb[170,171]. The LLE can be transformed to the dimensionless form in the following manner[116,164].

$$t' = \alpha\frac{t}{t_R}; \tau' = \tau\sqrt{\frac{2\alpha}{|\beta_2|L}}; E' = E\sqrt{\frac{\gamma L}{\alpha}}; \Delta = \frac{\delta_0}{\alpha};$$

$$D_k = \frac{L\beta_k}{\alpha k!}\left(\sqrt{\frac{2\alpha}{|\beta_2|L}}\right)^k; S = E_{in}\sqrt{\frac{\gamma L\theta}{\alpha^3}}$$

... (23)

After normalization, the LLE takes the following form,

$$\frac{\partial E'}{\partial t'} = \left[-1 - i\left(|E'|^2 - \Delta\right) + i\sum_{k\geq 2}D_k\left(i\frac{\partial}{\partial\tau'}\right)^k \right]E' + S$$ ... (24)

For a particular resonator dimension, given that the dispersion and nonlinear parameter remains constant, the solution of Eqn. (24) is solely controlled by the normalized pump power S and the normalized cavity detuning Δ. The soliton of Eqn. (24) is the DKS state given by $\sqrt{2\Delta}\,\text{sech}\sqrt{\Delta}\tau$. Eqn. (24) is revisited, with the conditions, $\frac{\partial E'}{\partial t'} = 0$ and $\frac{\partial E'}{\partial \tau'} = 0$. Clearly, the former results in stationary or steady state solution(s) of Eqn. (24), because the field evolution over the normalized "slow-time" t is equated to zero. On the

other hand, the latter indicates that the field evolution over the normalized "fast-time" τ is equated to zero. Since, the fast time corresponds to the frequency components of the produced DKS in the frequency domain, the condition $\frac{\partial E'}{\partial t'} = 0$ and $\frac{\partial E'}{\partial \tau'} = 0$ yields homogeneous solution(s) of Eqn. (24). When these two aforementioned conditions are imposed in the normalized LLE, the following cubic equation is arrived[111],

$$X = Y^3 - 2\Delta Y^2 + (\Delta^2 + 1)Y$$ ... (25)

Here, $X = |S|^2$ and $Y = |E|^2$ are representative of the normalized pump and intracavity powers respectively. For a constant CW input power Eqn. (25) illustrates the nonlinear Kerr tilt of the cavity resonance. The intracavity power Y (normalized with respect to the input power X) has been plotted for a range of Δ values (shown in Fig. 9(b)). Clearly three sets of intracavity field solutions can be evaluated from Eqn. (25) which includes: (i) Unconditionally homogeneous "stable" steady state solutions (shown by black circles); (ii) Unconditionally homogeneous "unstable" steady state solutions (shown by red asterisk); (iii) Conditionally homogenous stable solutions (shown by blue markers). Such solutions are associated with the phenomenon of Modulation Instability (MI) where a weak periodic perturbation develops on top of the steady state background both in the anomalous and normal dispersion regime[111] for micro-ring-resonators. These solutions are called "oscillatory" solutions. Experimentally the KFC and hence the DKS states are obtained by finely scanning the input pump frequency near the MRR resonance frequency so as to change the normalized detuning (Δ). This results in different DKS solutions. Three distinctive DKS solutions have been denoted by the yellow, violet, and green circles respectively. The physics behind the different analytical solutions of Eqn. (25) can be understood in the following manner. Initially the input CW pump power is low, and the solutions are inherently stable. Upon increasing the detuning, the cavity resonance enters the regime where it is red detuned with respect to the pump (corresponding to the yellow circle). Further increase in detuning leads to a purely unstable solution (indicated by the violet circle). An increase in detuning beyond this regime causes the cavity resonance to be blue-detuned with respect to the pump and stable DKS states are obtained. It should be

pointed out in this context that upon intracavity power build up, red-detuning resonance leads to increase in the local temperature gradient of the generated DKS state which causes the KFC to be unstable. The solution demarcated by the violet circle corresponds to the single DKS state. The theoretical demonstration of polarization dynamics of different soliton states have been comprehensively studied in the temporal domain in[172]. In this work, it has been observed that, in a birefringent optical fiber cavity, when the modes of one principal axis is excited, significant power gets coupled to the orthogonally polarized mode by the mechanism of cross phase modulation. Under such a situation, simple tweaking of the detuning parameter results in coexistence of three CS states: (i) CSs with MI, (ii) two identical CS, (iii) non-identical CS with different polarization properties. Here the numerical and theoretical studies have been conducted by solving the LLE and, the normalized fast-time, slow-time and detuning have been denoted by the symbols t, τ and σ, respectively. A theoretical study of DKS, using the LLE in the presence of dual pumping has been done by[117]. The generated DKS is formed on an oscillatory background, which is the characteristic of dual pumping. The generated DKS is immune to input jitters and third order dispersion induced temporal drift. Few results of[172,117] have been detailed in Fig. 10.

3.2 Stable and coherent KFC generation in MRR

Single DKS states generated from MRRs possess the ability to generate coherent and stable KFCs[149]. The single DKS states tend to position in the red-detuned side of the resonance where thermo-optical effects cause a major hindrance to access the stable soliton state[171,177]. The refractive index of the resonator gets modified on account of the thermal effects, which influences the circulating intracavity power within the MRR[178]. The thermal-time constant of on chip MRRs is quite fast due to which sustaining the stable single DKS state and hence KFC becomes really cumbersome. To ensure a fine control of the detuning between the pump and resonance mode in order to obtain a sustained and stable KFC from the MRR, several resonance tuning approaches have been proposed in literature. In[173] it has been demonstrated that operation in the cryogenic temperature regime facilitates direct access of the sustained stable DKS state through standard adiabatic frequency tuning of the pump laser. The experimental scheme is shown in Fig. 11(a).

This is predominantly because of the substantial reduction in the thermo-optic coefficient at cryogenic temperatures. Usage of integrated heaters have been proposed in[174,179] for fast thermal tuning of the resonance wavelength at a time scale which is shorter than the thermal relaxation time of the resonator. The scheme proposed in[174] has been illustrated in Fig. 11(b). Fine control over the electric current flowing through the heaters integrated within a Si_3N_4 MRR brings about proper sustenance of the single DKS state. The fast response time of the heaters play a important role for generation of stable KFC state. A very recent work[180] has reported the fabrication of integrated heaters buried deeply into the SiO_2 under-cladding of a Si_3N_4 MRR for efficient stabilization of KFCs. In[175] a novel stabilization mechanism has been proposed (Fig. 11(c)) where the
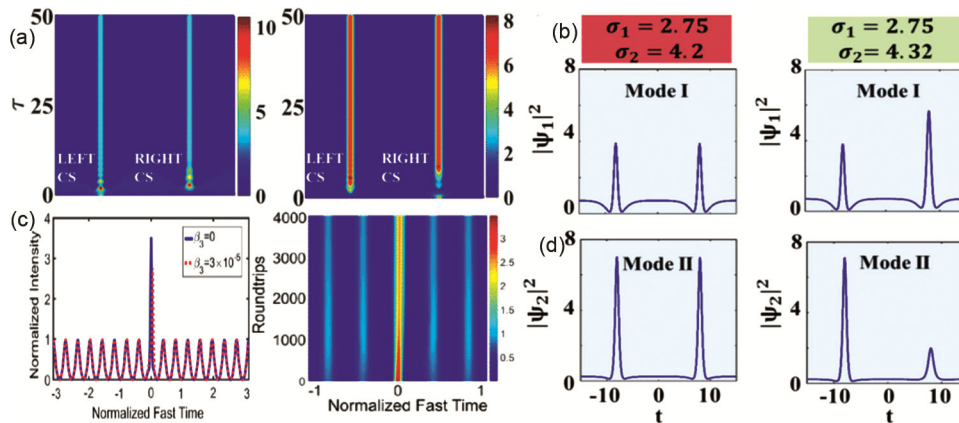

Fig. 10 — (a) Co-existence of CS in orthogonal polarization modes with different detuning mismatch σ_1= 2.75, σ_2= 4.2 for identical CS. (b) Power distribution for identical and non-identical coexisting CS for two orthogonal polarization modes at different detuning values.[172] (c) Dual pumped DKS, resilient towards third order dispersion induced temporal drift. (d) Evolution of field over multiple roundtrips, (c) and (d) are indicative of the oscillatory background.[117].
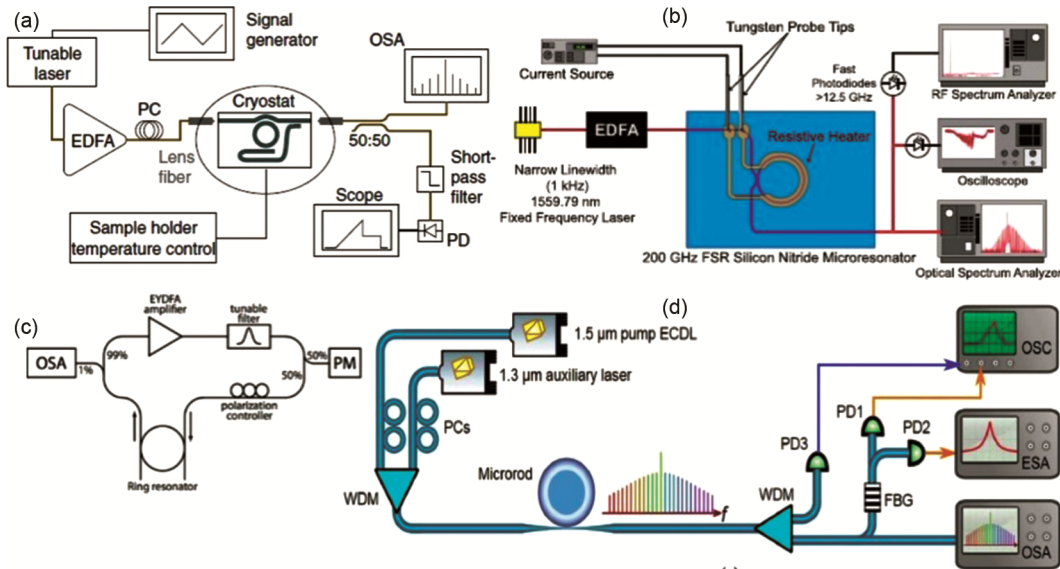
Fig. 11 — Different KFC stabilization schemes: (a) KFC generation at cryogenic temperatures[173], (b) Usage of integrated heaters for stabilization[174], (c) Placing the MRRin an external active fiber loop for stabilization[175], (d) usage of an auxiliary laser forstabilization[176]. Abbreviations used: Erbium doped fiber amplifier (EDFA), Polarization controller (PC), Optical Spectrum Analyzer (OSA), Photo-detector (PD), Phase Modulator(PM), Wavelength Division Multiplexer (WDM), Fiber Bragg Grating (FBG), Osilloscope(OSC), Electrical Spectrum Analyzer (ESA).
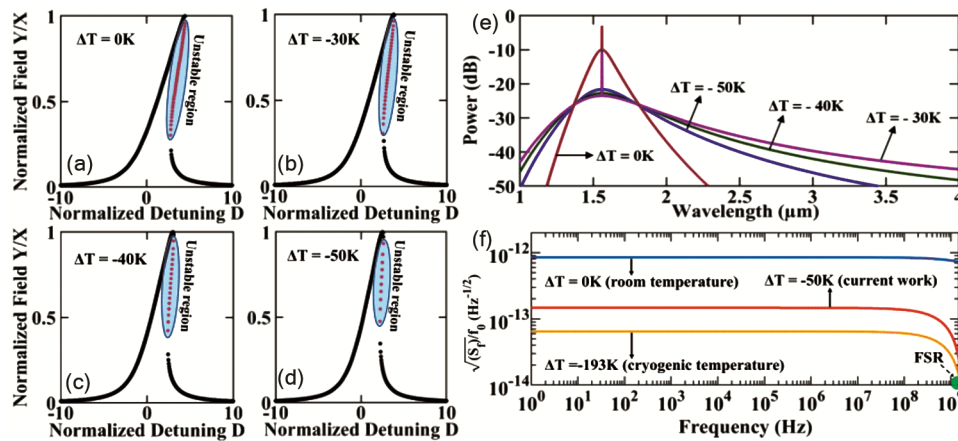

Fig. 12 (a)-(d) Decrease in the region of unstable solution upon decrease in temperature[183]. Here $\Delta T = Tr - Tl$ is the temperature gradient between the room (Tr) and chosen low temperature (Tl). (e) Increase in the bandwidth of the generated KFC at low temperatures. (f) Decrease in normalized spectral density of optical fluctuation $\sqrt{Sf/f0}$ at lower temperatures ($\Delta T = -50K, -193K$) compared to room temperature ($\Delta T = 0K$). The encircled frequency denotes the FSR of the cavity. (Images adapted from 183).

MRR has been placed in an external fiber loop cavity which possess optical gain.

The resonance of the MRR tends to synchronize with the fiber loop resonance and in turn is amplified. The MRR gets pumped by this amplified resonance which effectively masks the single DKS state within the stable blue-detuned regime of operation. Several other techniques like usage of single sideband modulators[181], phase modulation of the pump[182] have also been used to ensure generation of stable DKS

states. In[176] an auxiliary laser has been used along with the pump diode laser to passively stabilize the intra-cavity power of a fused Silica micro-rod resonator (Fig. 11(d)). Recently[164] it has been demonstrated through numerical simulations that the unstable solution of the LLE decreases at temperatures slightly lower than the room temperature (Fig. 12 (a)-(d)). Along with sustained single DKS state the bandwidth of the generated KFC also increases at low temperatures (Fig. 12(e)). The thermo-refractive noise
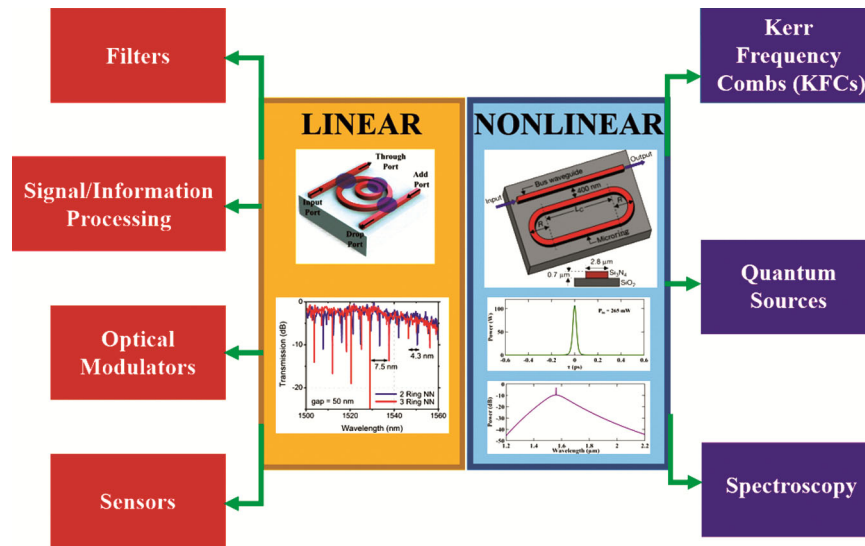
Fig. 13 — Application space of MRR, showcasing few and important domains.

of the KFC is quite low at lower temperatures than at the room temperature (Fig. 12(f)).

4 Conclusion and Outlook

Rapid and reliable exchange of information remained the principal driving force of the society since the latter half of the 20th century. Innumerable services and applications in the recent times ranging from traffic safety and guidance, Internet of Things (IOT), medical diagnosis, treatment and so on demand communication systems with high speed and large transmission capacity. The invention of optical fibres and its corresponding commercial usage from the 1970's and 90's have proved to be particularly effective to meet the ever-increasing demands of high data rate, reliability, and energy efficiency of communication systems, where the optical fibers have made its presence within data centers as well. However, the role of photonic technologies specifically at the chip-scale now gaining interest to meet several requirements whether it is for routing the data within a chip or sensing. Other than the celebrated optical waveguides as an optical interconnect, passive optical resonators gradually became an extremely important component for various applications such optical filters, mux and demux, modulator, sensors, and more recently in quantum light generation. With Silicon photonics being one of the most attractive technologies of the last decade on chip MRRs in the SOI platform have been vastly explored by researchers for a wide spectrum of applications. With an expected growth of 3.5 billion USD in the Silicon photonics market in the next five years, several leading photonics companies of the world that include AegiQ (UK), Cambridge Quantum Computing (UK), Hamamatsu photonics (Japan) etc. have started focussing on organized investment towards fabrication of Si-based MRRs for variety of applications in the communication sector.

Due to its importance in realizing on-chip applications and services, it is forecasted that MRRs can potentially evolve as a multi-billion-dollar investment sector by various foundries. Keeping in mind the importance of such a multifaceted optical element, in this review article, we attempted to provide a compact, yet comprehensive overview of MRRs. The diverse usage of MRRs for linear and nonlinear applications have been summarized in Fig. 13. In the domain of linear applications, MRRs have been exploited for designing fundamental and higher order filters, in signal and data processing, for realizing optical modulators and for on-chip sensing. Here, the usage of MRRs for filters and sensing applications have been discussed in detail. The idiosyncratic advantage of MRRs lie in the generation of on-chip coherent broadband KFCs which holds promise for replacing the existing power-hungry LASER based sources using WDM/DWDM, thereby cutting down cost effectively. Because of the unique ability of MRRs to confine the propagating electric field, nonlinear processes manifest effectively within them, which leads to the generation of robust single DKS state and hence KFCs. In this article the different material platforms utilized for generation of

KFCs, theoretical modelling of KFCs and the different schemes adopted by researchers to realize stable KFCs have been discussed in detail. The efficient manifestation of nonlinear optical processes in on-chip MRRs has been potentially exploited by researchers for generation of single photon sources, quantum logic operation *etc*.

References

1   Van V, *Optical microring resonators: theory, Techniques, and applications*. CRC Press, 2016.

2   Lefevre-Seguin`V & Haroche S, *Mater Sci Eng B*, 48 (1997) 53.

3   Braginsky V, Gorodetsky M & Ilchenko V, *Phys Lett A*, 137 (1989) 393.

4   Vernooy D, Furusawa A, Georgiades N P, Ilchenko V & Kimble H, *Phys Rev A*, 57 (1998) R2293.

5   Gorodetsky M L, Savchenkov A A & Ilchenko V S, *Opt Lett*, 21 (1996) 453.

6   Maker A J & Armani A M, *J Visual Exper*, 65 (2012) 4164.

7   Laine J-P, Tapalian C, Little B & Haus H, *Sens Actuators A: Phys*, 93 (2001) 1.

8   Sandoghdar V, Treussart F, Hare J, Lefevre-Seguin V, Raimond J-M & Haroche S, *Phys Rev A*, 54 (1996) R1777,.

9   Cai M, Painter O, Vahala K & Sercel P, *Opt Lett*, 25 (2000) 1430.

10 Wiersig J, *Phys Rev Lett*, 97 (2006) 253901.

11 Marcatili E, *Bell Syst Tech J*, 48 (1969) 2103.

12 Caruso L & Montrosset I, *J Lightwave Technol*, 21 (2003) 206.

13 Kokubun Y, Hatakeyama Y, Ogata M, Suzuki S & Zaizen N, *IEEE J Selec Top Quant Electron*, 11 (2005) 4.

14 Butt M, Khonina S & Kazanskiy N, *Laser Phys*, 29 (2019) 046208.

15 Grover R, Van V, T Ibrahim, Absil P, Calhoun L, Johnson F, Hryniewicz J & Ho P-T, *J Lightwave Technol*, 20 (2002) 872,.

16 Haldar R, Das S & Varshney S K, *J Lightwave Technol*, 31 (2013) 3976.

17 Cicek K & Cryan M, *J Opt*, 20 (2018) 085803.

18 Wu C-L, Chen B-T, Lin Y-Y, Tien W-C, Lin G-R, Chiu Y-J, Hung Y-J, Chu A-K & Lee C-K, *Opt Expr*, 23 (2015) 26268.

19 Rabus D G, *Integrated ring resonators*, Springer, 2007.

20 Bogaerts W, Heyn P D, Vaerenbergh T V, Vos K D, Selvaraja S K, Claes T, Dumon P, Bienstman P, Thourhout D V & Baets R, *Laser Photon Rev*, 6 (2012) 47.

21 Lee H S, Choi C-H, Beom-Hoan O, Lee S-G & Lee E-H, *Optical Fiber Commun Conf*, Optica Publishing Group, (2004) MF31.

22 Yariv A, *Electron Lett*, 36 (2000) 321.

23 Madsen C K & Zhao J H, *Optical filter design and analysis*, Wiley New York, 1999.

24 Jang J K, Klenner A, X Ji, Okawachi Y, Lipson M & Gaeta A L, *Nature Photon*, 12 (2018) 688.

25 Haldar R, Ummethala S, Sinha R K & Varshney S K, *J Soc Am B*, 38 (2021) 3743.

26 Soltani M, Yegnanarayanan S, Li Q & Adibi A, *IEEE J Quant Electron*, 46 (2010) 1158.

27 Barwicz T, Byun H, Gan F, Holzwarth C, Popovic M, Rakich P, Watts M, Ippen E, Kartner F, Smith H, *et al.*, *J Opt Network*, 6 (2007) 63.

28 Reed G T, Mashanovich G, Gardes F Y & Thomson D, *Nature Photon*, 4 (2010) 518.

29 Cocorullo G & Rendina I, *Electron Lett*, 1 (1992) 83.

30 Kauppinen L J, Abdulla S M, Krijnen G J, Pollnau M & Ridder R M de, *The European Conference on Lasers and Electro-Optics*, Optical Society of America, (2011) CE51.

31 Rakich P T, Popovic M A, Watts M R, Barwicz T, Smith H I & Ippen E P, *Opt Lett*, 31 (2006) 1241.

32 Asghari-Govar A, Andalib A, Zavvari M & Mohammadi P, *Optik*, 203 (2020) 163953.

33 Chung S, Nakai M & Hashemi H, *Opt Express*, 27 (2019) 13430.

34 Qiu C, Yang Y, Li C, Wang Y, Wu K & Chen J, *Sci Rep*, 7 (2017) 1.

35 Nielson G N, Seneviratne D, Lopez-Royo F, Rakich P T, Avrahami Y, Watts M R, Haus H A, Tuller H L & Barbastathis G, *IEEE Photon Technol Lett*, 17 (2005) 1190.

36 Haldar R, Mishra V, Koos C, Freude W & Varshney S K, *Optica Publishing Group*, (2016) 6.

37 Haldar R, Banik A D & Varshney S K, *Optics Express*, 22 (2014) 22411.

38 Jinguji K & Oguma M, *J Lightwave Technol*, 18 (2000) 252.

39 Little B, Chu S, Absil P, Hryniewicz J, Johnson F, Seiferth F, Gill D, Van V, King O & Trakalo M, *IEEE Photon Technol Lett*, 16 (2004) 2263.

40 Little B E, Chu S T, Haus H A, Foresi J & Laine J-P, *J Lightwave Technol*, 15 (1997) 998.

41 Yariv A, Xu Y, Lee R K & Scherer A, *Opt Lett*, 24 (1999) 711.

42 Hryniewicz J, Absil P, Little B, Wilson R & Ho P-T, *IEEE Photon Technol Lett*, 12 (2000) 320.

43 Watts M R, Barwicz T, Popovic M, Rakich P T, Socci L, Ippen E P, Smith H I & Kaertner F, *Conference on Lasers and Electro-Optics*, Optica Publishing Group, (2005) 3.

44 Xia F, Sekaric L & Vlasov Y, *Nature Photon*, 1 (2007) 65.

45 Ye Y-H, Ding J, Jeong D-Y, Khoo I & Zhang Q, *Phys Rev E*, 69 (2004) 056604.

46 Xiao S, Khan M H, Shen H & Qi M, *Opt Express*, 15 (2007) 14765.

47 Villers S B, Hould D & Shi W, *2019 Optical Fiber Communications Conference and Exhibition (OFC)*, IEEE, (2019) 1.

48 Gan F, Barwicz T, Popovic M, Dahlem M, Holzwarth C, Rakich P, Smith H, Ippen E & Kartner F, *2007 Photonics in Switching*, (2007) 67.

49 Xia F, Rooks M, Sekaric L & Vlasov Y, *Opt Express*, 15 (2007) 11934.

50 Padmaraju K & Bergman K, *Nanophotonics*, 3 (2014) 269.

51 Jayatilleka H, Murray K, Guillen-Torres M A´,´ Caverley M, Hu R, Jaeger N A, Chrostowski L & Shekhar S, *Optics Express*, 23 (2015) 25084.

52 Mak J C, Sacher W D, Xue T, Mikkelsen J C, Yong Z & Poon J K, *IEEE J Quant Electron*, 51 (2015) 1.

53 Popovic M, Theory and design of high-index-contrast microphotonic circuits, Ph.D. dissertation, Massachusetts Institute of Technology, 2008.

54 Bienstman P, Six E, Roelens A, Vanwolleghem M & Baets R, *IEEE Photon Technol Lett*, 14 (2002) 164.

55 Vlasov Y A & McNab S J, *Opt Express*, 12 (2004) 1622.

56 Morichetti F, *Photonic Microresonator Research and Applications*, Springer, (2010) 61.

57 Oda K, Takato N & Toba H, *J Lightwave Technol*, 9 (1991) 728.

58 Van V, Little B E, Chu S T & Hryniewicz J V, *The 17th Annual Meeting of the IEEE Lasers and Electro-Optics Society IEEE*, 2 (2004) 571.

59 Griffel G, *IEEE Photon Technol Lett*, 12 (2000) 1642.

60 Barbarossa G, Matteo A M & Armenise M N, *J Lightwave Technol*, 13 (1995) 148.

61 Dey S B, Mandal S & Jana N N, *Appl Opt*, 51 (2012) 6901.

62 Yanagase Y, Suzuki S, Kokubun Y & Chu S T, *J Lightwave Technol*, 20 (2002) 1525.

63 Boeck R, Shi W, Chrostowski L & Jaeger N, *IEEE Photon J*, 5 (2013) 2202511.

64 Geuzebroek D, Klein E, Kelderman H, Tan F, Klunder D & Driessen A, *Proceedings Symposium IEEE/LEOS Benelux Chapter*, Vrije Universiteit Amsterdam Amsterdam, (2002) 155.

65 Dey S & Mandal S, *Opt Eng*, 50 (2011) 084601.

66 Xiao S, Khan M H, Shen H & Qi M, *J Lightwave Technol*, 26 (2008) 228.

67 Urbonas D, Balcytis A, Gabalis M, Vaskevičius K, Naujokaite G, Juodkazis S & Petruskevičius R, *Opt Lett*, 40 (2015) 2977.

68 Wu J, Moein T, Xu X, Ren G, Mitchell A & Moss D J, *Apl Photon*, 2 (2017) 056103.

69 Bag S K & Varshney S K, *J Opt Soc Am B*, 38 (2021) 1669.

70 Chao C-Y & Guo L J, *Appl Phys Lett*, 83 (2003) 1527.

71 Acha N D, Socorro-Leranoz A B, Elosua C, & Matías I R, *Biosensors*, 11 (2021)197.

72 Chao C-Y & Guo L J, *J Lightwave Technol*, 24 (2006) 1395.

73 Ramachandran A, Wang S, Clarke J, Ja S, Goad D, Wald L, Flood E, Knobbe E, Hryniewicz J, Chu S, *et al.*, *Biosens Bioelectron*, 23 (2008) 939.

74 Yan H, Huang L, Xu X, Chakravarty S, Tang N, Tian H & Chen R T, *Opt Express*, 24 (2016) 29724.

75 Yalcin A, Popat K C, Aldridge J C, Desai T A, Hryniewicz J, Chbouki N, Little B E, King O, Van V, Chu S, *et al.*, *IEEE J Select Top Quant Electron*, 12 (2006) 148.

76 Vos K D, Bartolozzi I, Schacht E, Bienstman P & Baets R, *Opt Express*, 15 (2007) 7610.

77 Cardenosa-Rubio M C, Robison H M & Bailey R C, *Curr Opin Environ Sci Health*, 10 (2019) 38.

78 Matsuura S, Yamasaku N, Nishijima Y, Okazaki S & Arakawa T, *Sensors*, 20 (2019) 96.

79 Kishikawa H, Sato M, Goto N, Yanagiya S-I, Kaito T & Liaw S K, *Jpn J Appl Phys*, 8, (2019) SJJD05.

80 Yebo N A, Taillaert D, Roels J, Lahem D, Debliquy M, Thourhout D V & Baets R, *IEEE Photon Technol Lett*, 21 (2009) 960.

81 Qiao Y, Tao J, Chen C-H, Qiu J, Tian Y, Hong X & Wu J, *Micromachines*, 8 (2017) 160.

82 Fu D, Chung J, Liu Q, Raziq R, Kee J S, Park M K, Valiyaveettil S & Lee P, *Sens Actuators B: Chem*, 257 (2018) 136.

83 Hajikhanloo A S, Sarraf M J, Rostami A & Dolatyari M, Micro Ring Resonator Based Co2 Gas Sensor using Pbse Quantum Dots, 2021.

84 Eisner L, Wilhelm I, Flachenecker G, Hurttlen J & Schade W, *Sensors*, 19 (2019) 3909.

85 S Borjian, Saunders J, X Wu, Crudden C M, Loock H-P, *et al.*, *Appl Industr Opt: Spectros, Imag Metrol*, Optica Publishing Group, (2015) AIM2D.

86 Chauvin D, Bell J, Leray I, Ledoux-Rak I & Nguyen C T, *Sens Actuators B: Chem*, 280 (2019) 77.

87 Stievater T H, Pruessner M W, Park D, Rabinovich W S, McGill R A, Kozak D A, Furstenberg R, Holmstrom S A & Khurgin J B, *Opt Lett*, 39 (2014) 969.

88 Zhang P, Ding Y & Wang Y, *Optik*, 171 (2018) 642.

89 Shia W W & Bailey R C, *Anal Chem*, 85 (2013) 805.

90 Chen Y, Liu Y, Shen X, Chang Z, Tang L, Dong W-F, Li M & He J-J, *Sensors*, 15 (2015) 1558.

91 Bahadoran M, Noorden A F A, Mohajer F S, Mubin M H A, Chaudhary K, Jalil M A, Ali J & Yupapin P, *Artificial cells, Nanomed Biotechnol*, 44 (2016) 315.

92 McClellan M S, Domier L L & R Bailey C, *Biosens Bioelectron*, 31 (2012) 388.

93 Estrada I, Burlingame R, Wang A, Chawla K, Grove T, Wang J, Southern S, Iqbal M, Gunn L & Gleeson M, *Advances in Global Health through Sensing Technologies*, 9490 (2015) 36.

94 Beusink J B, A Lokate M, Besselink G A, Pruijn G J & Schasfoort R B, *Biosens Bioelectron*, 23 (2008) 839.

95 Zhuo Y, Hu H, Chen W, Lu M, Tian L, Yu H, Long K D, Chow E, King W P, Singamaneni S, *et al.*, *Analyst*, 139 (2014) 1007.

96 Li H, Luo X, Du C, Chen X & Fu Y, *Sens Actuators B: Chem*, 134 (2008) 940.

97 Vollmer F, Arnold S & Keng D, *Proc Nat Acad Sci*, 105 (2008) 20701.

98 Li X, Zhang Z, Qin S, Wang T, Liu F, Qiu M & Su Y, *Appl Opt*, 48 (2009) F90.

99 Zhang W, Li W & Yao J, *Opt Lett*, 41 (2016) 2474.

100 Bag S K, Sinha R K, Wan M & Varshney S, *J Phys D: Appl Phys*, 54 (2021) 16LT01.

101 Biswas U, Rakshit J K, Das J, Bharti G K, Suthar B, Amphawan A & Najjar M, *Silicon*, 13 (2021) 885.

102 Hu C, Shi Y, Zhou T, Xu C & Zhu A, *Silicon*, 14 (2022) 5847.

103 Wang C-T, Wang C-Y, Yu J-H, Kuo I-T, Tseng C-W, Jau H-C, Chen Y-J & Lin T-H, *Opt Express*, 24 (2016) 1002.

104 Bhola B, Song H-C, Tazawa H & Steier W H, *IEEE Photon Technol Lett*, 17 (2005) 867.

105 Bhola B & Steier W H, *IEEE Sens J*, 7 (2007) 1759.

106 Chao C-Y, Ashkenazi S, Huang S-W, O'Donnell M & Guo L J, *IEEE Trans Ultrason, Ferroelectr Freq Control*, 54 (2007) 957.

107 Maxwell A, Huang S-W, Ling T, Kim J-S, Ashkenazi S & Guo L J, *IEEE J Select Top Quan Electron*, 14 (2008) 191.

108 Dong B, Chen S, Zhang Z, Sun C & Zhang H F, *Opt Lett*, 39 (2014) 4372.

109 Li H, Dong B, Zhang Z, Zhang H F & Sun C, *Sci Rep*, 4 (2014) 1.

110 Agrawal G P, *Nonlinear Science at the Dawn of the 21st Century*. Springer, (2000) 195.

111 Grelu P, *Nonlinear optical cavity dynamics: from microresonators to fiber lasers*, John Wiley & Sons, 2015.

112 T Kippenberg J, Holzwarth R & Diddams S A, *Science*, 332 (2011) 555.

113 Scroggie A, W Firth, McDonald G, Tlidi M, Lefever R & Lugiato L A, *Chaos, Solitons Fractals*, 4 (1994) 1323.

114 Del'Haye P, Schliesser A, Arcizet O, Wilken T, Holzwarth R & Kippenberg T J, *Nature*, 450 (2007) 1214.

115 Rotschild C, Alfassi B, Cohen O & Segev M, *Nature Phys*, 2 (2006) 769.

116 Leo F, Coen S, Kockaert P, Gorza S-P, Emplit P & Haelterman M, *Nature Photon*, 4 (2010) 471.

117 Roy A, Haldar R & Varshney S K, *J Lightwave Technol*, 36 (2018) 5807.

118 Kartashov Y, Alexander O & Skryabin D, *Opt Express*, 25 (2017) 11550.

119 Matsko A B, Liang W, Savchenkov A A, Eliyahu D & Maleki L, *Opt Lett*, 41 (2016) 2907.

120 Ludlow A D, Boyd M M, Ye J, Peik E & Schmidt P O, *Rev Mod Phys*, 87 (2015) 637.

121 Drake T E, Briles T C, Stone J R, Spencer D T, Carlson D R, Hickstein D D, Li Q, Westly D, K Srinivasan, Diddams S A, *et al.*, *Phys Rev X*, 9 (2019) 031023.

122 Holzwarth R, Udem T, Hansch T W, Knight J, Wadsworth W & Russell P S J, *Phys Rev Lett*, 85 (2000) 2264.

123 Spencer D T, Drake T, Briles T C, Stone J, Sinclair L C, Fredrick C, Li Q, Westly D, Ilic B R, Bluestone A, *et al.*, *Nature*, 557 (2018) 81.

124 Fortier T M, Kirchner M S, Quinlan F, Taylor J, Bergquist J, Rosenband T, Lemke N, Ludlow A, Jiang Y, Oates C, *et al.*, *Nature Photon*, 5 (2011) 425.

125 Foltynowicz A, Masłowski P, Ban T, Adler F, Cossel K, Briles T & Ye J, *Faraday Discuss*, 150 (2011) 23.

126 Levy J S, Gondarenko A, Foster M A, Turner-Foster A C, Gaeta A L & Lipson M, *Nature Photon*, 4 (2010) 37.

127 Razzari L, Duchesne D, Ferrera M, Morandotti R, Chu S, Little B E & Moss D J, *Nature Photonics*, 4 (2010) 41.

128 Savage N, *Nature Photon*, 3 (2009) 114.

129 Ferdous F, Miao H, Leaird D E, Srinivasan K, Wang J, Chen L, Varghese L T & Weiner A M, *Nature Photon*, 5 (2011) 770.

130 Del'Haye P, Herr T, Gavartin E, Gorodetsky M L, Holzwarth R & Kippenberg T J, *Phys Rev Lett*, 107 (2011) 063901.

131 Okawachi Y, Saha K, Levy J S, Wen Y H, Lipson M & Gaeta A L, *Opt Lett*, 36 (2011) 3398.

132 Leuthold J, Koos C & Freude W, *Nature Photon*, 4 (2010) 535.

133 M Foster A, Salem R, Geraghty D F, Turner-Foster A C, Lipson M & Gaeta A L, *Nature*, 456 (2008) 81.

134 Salem R, Foster M A, Turner A C, Geraghty D F, Lipson M & Gaeta A L, "*Nature Photon*, 2 (2008) 35.

135 Monat C, Corcoran B, Pudo D, Ebnali-Heidari M, Grillet C, Pelusi M D, Moss D J, Eggleton B J, White T P,

O'Faolain L, *et al.*, *IEEE J SelectTop Quant Electron*, 16 (2009) 344.

136 Rong H, Jones R, Liu A, Cohen O, Hak D, Fang A & Paniccia M, *Nature*, 433 (2005) 725.

137 Foster M A, Turner A C, Sharping J E, Schmidt B S, Lipson M & Gaeta A L, *Nature*, 441 (2006) 960.

138 Kuyken B, Liu X, Roelkens G, Baets R, Osgood R M & Green W M, *Opt Lett*, 36 (2011) 4401.

139 Zlatanovic S, Park J S, Moro S, Boggio J M C, Divliansky I B, Alic N, Mookherjea S & Radic S, *Nature Photon*, 4 (2010) 561.

140 Liu X, Osgood R M, Vlasov Y A & Green W M, *Nature Photon*, 4 (2010) 557.

141 Singh N, Hudson D D, Yu Y, Grillet C, Jackson S D, Bedoya A C, Read A, Atanackovic P, Duvall S G, Palomba S, *et al.*, *Optica*, 2 (2015) 797.

142 Griffith A G, Lau R K, Cardenas J, Okawachi Y, Mohanty A, Fain R, Lee Y H D, Yu M, Phare C T, Poitras C B, *et al.*, *Nature Commun*, 6 (2015) 1.

143 Pafchek R, Tummidi R, Li J, Webster M, Chen E & Koch T, *Appl Opt*, 48 (2009) 958.

144 Haldar R, Roy A, Mondal P, Mishra V & Varshney S K, *Phys Rev A*, 99 (2019) 033848.

145 Moss D J, Morandotti R, Gaeta A L & Lipson M, *Nature Photon*, 7 (2013) 597.

146 Duchesne D, Ferrera M, Razzari L, Morandotti R, Little B E, Chu S T & Moss D J, *Opt Express*, 17 (2009) 1865.

147 Herr T, Hartinger K, Riemensberger J, Wang C, Gavartin E, Holzwarth R, Gorodetsky M & Kippenberg T, *Nature Photon*, 6 (2012) 480.

148 Johnson A R, Okawachi Y, Levy J S, Cardenas J, Saha K, Lipson M & Gaeta A L, *Opt Lett*, 37 (2012) 875.

149 Saha K, Okawachi Y, Shim B, Levy J S, Salem R, Johnson A R, Foster M A, Lamont M R, Lipson M & Gaeta A L, *Opt Express*, 21 (2013) 1335.

150 Herr T, Brasch V, Jost J D, Wang C Y, Kondratiev N M, Gorodetsky M L & Kippenberg T J, *Nature Photon*, 8 (2014) 145.

151 Peccianti M, Pasquazi A, Park Y, Little B E, Chu S T, Moss D J & Morandotti R, *Nature Commun*, 3 (2012) 1.

152 Pasquazi A, Caspani L, Peccianti M, Clerici M, Ferrera M, Razzari L, Duchesne D, Little B E, Chu S T, Moss D J *et al.*, *Opt Express*, 21 (2013) 13333.

153 Levy J S, Foster M A, Gaeta A L & Lipson M, *Opt Express*, 19 (2011) 11415.

154 Ikeda K, Saperstein R E, Alic N & Fainman Y, *Opt Express*, 16 (2008) 12987.

155 Luke K, Dutt A, Poitras C B & Lipson M, *Opt express*, 21 (2013) 22829.

156 Riemensberger J, K Hartinger, T Herr, Brasch V, Holzwarth R & Kippenberg T J, *Opt Express*, 20 (2012) 27661.

157 Luke K, Okawachi Y, Lamont M R, Gaeta A L & Lipson M, *Opt Lett*, 40 (2015) 4823.

158 Pfeiffer M H, Herkommer C, Liu J, Guo H, Karpov M, Lucas E, Zervas M & Kippenberg T J, *Optica*, 4 (2017) 684.

159 Liu Y, Y Xuan, Xue X, Wang P-H, Chen S, Metcalf A J, Wang J, Leaird D E, Qi M & Weiner A M, O*ptica*, 1 (2014) 137.

160 Saha M, Roy S & Varshney S K, *Phys Rev A*, 104 (2021) 033514.

161 Wang Y, Shi L, Wu W, Ming X, Sun Q, Wang L & Zhao W, *Appl Opt*, 61 (2022) 2629.

162 Ji H, Geng Z, Cheng W, Yu Z, Wu P, Li Y & Zhao Q, *arXiv preprint arXiv:*2209.15354, (2022).

163 Kim C, Ye C, Zheng Y, Semenova E, Yvind K & Pu M, *IEEE J Select Top Quant Electron*, (2022).

164 Kar S, Saha M, Bag S K, Sinha R K, Sharma S, Singhal S & Varshney S K, *Phys Rev A*, 106 (2022) 013517.

165 Dean K, *Waves and fields in optoelectronics*, Prentice-hall series in solid state physical electronics, (1984).

166 Lugiato L A & Lefever R, *Phys Rev Lett*, 58 (1987) 2209.

167 Ikeda K, *Opt commun*, 30 (1979) 257.

168 Ikeda K, Daido H & Akimoto O, *Phys Rev Lett*, 45 (1980) 709.

169 M Haelterman, Trillo S & Wabnitz S, *Opt Commun*, 91 (1992) 401.

170 Coen S & Erkintalo M, *Opt Lett*, 38 (2013) 1790.

171 Godey C, Balakireva I V, Coillet A & Chembo Y K, *Phys Rev A*, 89 (2014) 063814.

172 Saha M, Roy S & Varshney S K, *Phys Rev A*, 101 (2020) 033826.

173 G Moille, X Lu, Rao A, Li Q, Westly D A, Ranzani L, Papp S B, Soltani M & Srinivasan K, *Phys Rev Appl*, 12 (2019) 034057.

174 Joshi C, Jang J K, Luke K, Ji X, Miller S A, A Klenner, Okawachi Y, Lipson M & Gaeta A L, *Opt Lett*, 41 (2016) 2565.

175 Pasquazi A, Caspani L, Peccianti M, Clerici M, Ferrera M, Razzari L, Duchesne D, Little B E, Chu S T, Moss D J, *et al.*, *Optics Express*, 21 (2013) 13333.

176 Zhang S, Silver J M, Bino L D, Copie F, Woodley M T, Ghalanos G N, Svela A Ø, Moroney N & Del'Haye P, *Optica*, 6 (2019) 206.

177 Carmon T, Yang L & Vahala K J, *Opt Express*, 12 (2004) 4742.

178 Y Deng, Liu F, Leseman Z C & Hossein-Zadeh M, *Opt Express*, 21 (2013) 4653.

179 Xue X, Xuan Y, Liu Y, Wang P-H, Chen S, Wang J, Leaird D E, Qi M & Weiner A M, *Nature Photon*, 99 (2015) 594.